Received 23 July 2025; accepted 18 August 2025. Date of publication 25 August 2025; date of current version 9 September 2025.

Digital Object Identifier 10.1109/OJCOMS.2025.3602090

LEO Satellite Beam Hopping for Power Consumption Minimization at Different Elevation Angles

AGNES FASTENBAUER [1,2,3] (Member, IEEE), YOUNES EL HADFI [4], MEGUMI KANEKO [2,5] (Senior Member, IEEE), PHILIPP SVOBODA [1,3] (Senior Member, IEEE), AND MARKUS RUPP [3] (Fellow, IEEE)

[1]Christian Doppler Laboratory for Digital Twin Assisted AI for Sustainable Radio Access Networks, TechnischeUniversitat Wien, 1040 Vienna, Austria
[2]Information Systems Architecture Science Research Division, National Institute of Informatics, Chiyoda City 101-8430, Tokyo, Japan
[3]Institute of Telecommunications, TU Wien, 1040 Wien, Austria
[4]ISAE-SUPAERO, Université de Toulouse, 31055 Toulouse, France
[5]Department of Computer Science, The University of Tokyo, Bunkyo City 113-0033, Tokyo, Japan

CORRESPONDING AUTHOR: A. FASTENBAUER (e-mail: agnes.fastenbauer@tuwien.ac.at)

This work was supported in part by the TU Wien Bibliothek through its Open Access Funding Program; in part by the Christian Doppler Laboratory for Digital Twin assisted AI for sustainable Radio Access Networks; in part by the Austrian Federal Ministry for Digital and Economic Affairs, the National Foundation for Research, Technology and Development and the Christian Doppler Research Association; in part by the NII-TU Wien MoU Grant funded by NII, the Grant-in-Aid for Scientific Research (Kakenhi) from the Ministry of Education, Science, Sports, and Culture of Japan, under Grant 22KK0156; and in part by the JST ASPIRE under Grant JPMJAP2325.

ABSTRACT Low Earth orbit (LEO) satellite communication promises to bridge the digital divide. As satellite payload is limited, methods such as beam hopping techniques are necessary to ensure that the scarce resources are used efficiently. Current literature lacks sufficient studies on the effects of LEO satellite movement on the system behavior. To help bridge this gap, this paper analyzes the performance of beam hopping techniques in dependence on the elevation angle. We consider downlink transmission of a multi-beam LEO satellite operating in the K_a-band (30 GHz). An established beam hopping scheme from geosynchronous equatorial orbit (GEO) satellite systems is adapted to LEO systems and an interference-aware greedy beam hopping algorithm is developed. The two proposed algorithms are compared to three benchmarks (exhaustive search, random beam hopping, and full illumination) under consideration of different satellite elevation angles. Simulation results show that the interference-aware proposed method performs close to optimal and outperforms the GEO-adapted scheme, especially at low elevation angles. The results confirm that a significant power consumption reduction at the satellite can be achieved with beam hopping techniques, especially in networks under low utilization.

INDEX TERMS 6G, beam hopping, beam hopping pattern, Ka band, LEO, multi-beam satellite, non-terrestrial network, optimization, satellite communication, wireless communication.

I. INTRODUCTION

A. BACKGROUND

GEOGRAPHICALLY remote regions, both on land and water, lack coverage from mobile networks as network deployment costs exceed return expectations. This contributes to the global digital divide. One technology that can help bridge the gap between well-connected users and those cut off from the Internet is low Earth orbit (LEO) satellite communication [1], which is intended to be combined with terrestrial networks in order to offer full and seamless coverage anywhere in the world [2].

Contrary to the already well-established geosynchronous equatorial orbit (GEO) satellite communication, LEO satellite communication promises lower latency due to the proximity to Earth. One of the LEO satellite networks in development, *Starlink*, promises to deliver a median latency of 20 ms and delivers latency around 50 ms [3]. For comparison, up to 150 ms delay is acceptable for voice transmission according to the International Telecommunication Union (ITU) [4]. The low latency and a reduction in launching costs led to the rise of several LEO satellite networks.

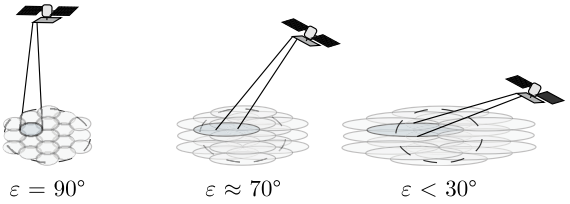

FIGURE 1. Distortion of the satellite footprint with changing elevation angle. The shape of the beam footprint - depicted as a blue ellipse - is stretched when the satellite moves towards lower elevation angles.

The fast movement of the LEO satellites, at around 7800 m/s, introduces new challenges into satellite systems, namely strong Doppler shifts, high handover rates, and a distortion of the beam footprint on the ground [5]. The distortion of the footprint on ground is due to the changing elevation angle of the satellite, where the projection of the beam footprint pattern is distorted when the satellite moves to more acute angles with respect to the coverage region marked with a dashed circle in Fig. 1. Whereas the Doppler shift can be estimated and compensated [6], [7], [8], the footprint distortion affects transmission, especially if handover rates are reduced by maintaining the connection to the serving satellite at low satellite elevation angles. The system behavior under different elevation angles is analyzed in [9].

Because LEO satellites are usually smaller than conventional GEO satellites, it is vital to meet the limitations of the satellite's onboard power constraint. To this aim, beam hopping techniques are employed. In beam hopping, the satellite's beams are activated and deactivated on a short time scale to minimize the system's power consumption and resource requirements while serving the users in the serving region. Beam hopping schemes are applied in GEO satellite systems [10], [11]. However, the elevation-dependence of the system behavior has mostly been neglected in literature on LEO satellite beam hopping schemes [12], [13], [14].

A challenge present in both GEO and LEO multi-beam satellites is strong co-channel interference. A user receives the signal from all beams through the same physical channel. One of the satellite beams transmits the desired signal intended for the user, the other beams transmit data intended for other users and are treated as interference. As the transmitters of the beams are co-located on the satellite and no scattering components are present in the vicinity of the transmitter, the channel fading experienced by all signals, desired and interfering, is identical [5], [15], [16]. As the interfering signal experiences the same physical channel conditions, it is called co-channel interference [5].

B. RELATED WORK

Since beam hopping has been proven to enhance system utilization [17], several works have proposed beam hopping schemes aimed at optimizing different network metrics. For GEO systems, [18] presents and compares several conventional beam hopping schemes that maximize capacity and user satisfaction, while [19] and [20] present deep reinforcement learning beam hopping schemes that maximize throughput and capacity, respectively. In [10], a system is developed that minimizes the precoding effort by reducing the interference in the system through beam hopping.

In LEO satellite systems, minimizing the system latency is often an additional optimization goal to throughput maximization: [21] proposes a determinant point process algorithm, [22] uses a deep reinforcement learning approach, [23] a multi-agent reinforcement learning approach, and [24] presents a cooperative multi-agent proximal policy optimization algorithm.

Beam hopping energy consumption in a code division multiple access system is explored in [14]. The authors of [13] explore sum-rate maximization in LEO satellite systems.

In [12], a beam hopping pattern that minimizes the transmit power is proposed for systems with a small (2×4) transmit antenna array. We propose a model for large antenna arrays, considering a 32×32 antenna configuration per beam. A heterogeneous graph based solution optimizes the energy efficiency of a LEO system in [25]. However, the scheme requires training data and time and a large number of training episodes to converge, while our proposed models operate with data present in the system and does not require training.

Furthermore, the presented methods in this section do not consider different satellite elevation angles to evaluate the performance of the beam hopping pattern algorithms even though the system's behavior changes significantly with the elevation angle, as shown in [9]. By contrast, this paper evaluates the proposed and benchmark schemes at three representative elevation angles to obtain a complete picture of the algorithms' performance.

C. CONTRIBUTIONS

This paper investigates beam hopping pattern algorithms that minimize the power consumption at the satellite in consideration of the satellite elevation angle. We consider the downlink transmission of a multi-beam LEO satellite operating in the K_a-band [26]. The system is sketched in Fig. 2. The satellite beams can be activated and deactivated on a short time scale in the order of milliseconds, which allows to employ beam hopping schemes that reduce the power consumption.

Two beam hopping algorithms are proposed. First, an integer linear programming (ILP) optimization algorithm is developed. The algorithm is adapted from a GEO satellite system in [10]. The non-convex power consumption minimization problem is simplified with the introduction of an interference estimation scheme that linearizes the constraint function from the optimization variable. With the modified user rate constraint, the resulting problem is an ILP problem that can be solved with conventional solvers. Second, an interference-aware greedy algorithm with low computational complexity is proposed. Additionally, to compare the power consumption of the different beam hopping

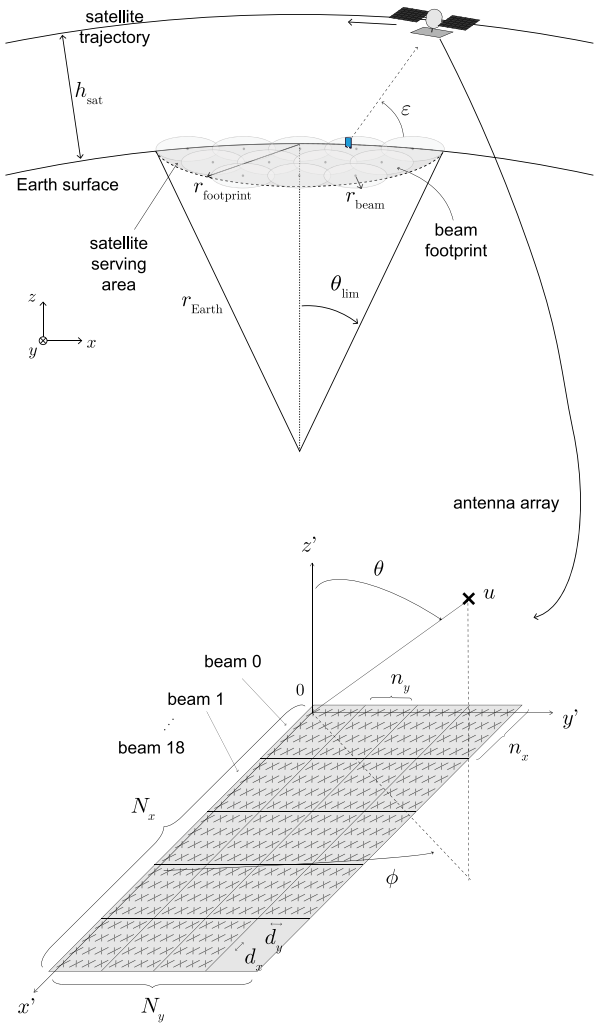

FIGURE 2. Sketch of the satellite system - distances are not at scale. The satellite moves over the satellite serving area. The elevation angle ε changes over the satellite's trajectory.

algorithms, a power consumption model for downlink multi-beam satellite transmission is developed based on current literature. The model evaluates the power consumption of the satellite.

The proposed beam hopping patterns are compared to three benchmarks in terms of power consumption and outage rates. The benchmarks are an exhaustive search over all valid beam patterns, a random algorithm, and a fully illuminated beam pattern. Results of the performance comparison through Monte Carlo simulations of a realistic system model based on [9] show that the proposed interference-aware greedy algorithm performs close to optimal exhaustive search, while the algorithm adapted from GEO systems shows higher outage rates, especially at medium and low elevation angles.

It should be noted that our previous work in [9] evaluates the link quality in the satellite serving area in terms of unprecoded signal to interference and noise ratio (SINR) over different elevation angles. By contrast, in order to evaluate the throughput of different beam hopping schemes, this paper extends the system model from [9] with a round robin sub-band allocation scheme and a minimum mean squared error (MMSE) precoding scheme. This allows the accurate evaluation of the theoretical upper bound of the user rate, providing a realistic estimation of key system performance indicators, such as the outage and sum rate. The developed power consumption model allows the evaluation of the satellite's power consumption under different beam hopping schemes.

The contributions of this paper can be summarized as follows:

1) *Adaptation of GEO beam hopping pattern to LEO systems:* in particular, average capacity estimation in [10, Algorithm 2] is adapted to LEO systems as an average interference estimation to linearize the dependency on the optimization variable of the side constraint.
2) *Development of interference-aware greedy heuristic beam hopping pattern algorithm:* a computationally efficient beam hopping pattern scheme is developed that minimizes the inter-beam interference.
3) *Development of a power consumption model for downlink LEO satellite communications:* to model the power consumption at the transmitter of a downlink multi-beam satellite transmission, the power consumption models presented in [27], [28], [29], [30] are combined. Existing literature focuses on the power consumption at terrestrial transmitters and receivers and, to the best of our knowledge, does not provide a power consumption model for satellite communications.
4) *Performance comparison of proposed beam hopping pattern algorithms with benchmark algorithms:* the simulation results demonstrate that the proposed interference-aware greedy heuristic performs close to the optimal exhaustive search benchmark and outperforms the other benchmarks in terms of power consumption and throughput, at all elevation angles and under different network loads.
5) *Provision of open-source Python implementation* for regeneration of results and performance analysis with varying parameters [31].

D. PAPER OUTLINE

The remainder of the paper is organized as follows: the system model is described in Section II with the introduction of the adapted power consumption model in Section II-I. The optimization problem to solve is formulated in Section III. Then, the beam hopping algorithms are defined in Section IV, and their performance is evaluated at three representative elevation angles in Section V. Section VI discusses limiting assumptions and important future perspectives. Finally, Section VII concludes this paper and directions for future work are given.

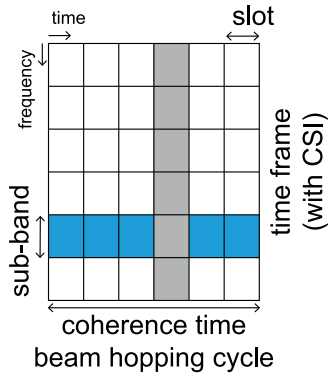

FIGURE 3. Transmission resources. The available bandwidth is divided into sub-bands that are assigned to users. Beams are activated or deactivated in each slot in order to serve all users while maintaining the resource utilization low.

II. MULTI-BEAM SATELLITE SYSTEM MODEL

This section defines the system model. The downlink transmission in a multi-beam LEO satellite system operating in the K_a-band is considered. The scenario is sketched in Fig. 2. The chosen setup extends the system model in [9] with a sub-band allocation scheme, a digital precoder, beam hopping schemes, and a model of the power consumption at the satellite.

A. NETWORK GEOMETRY

The satellite traverses a circular trajectory at altitude h_{sat} above the ground and serves a fixed satellite serving area of radius $r_{\text{footprint}}$ on the surface of the Earth.

In this serving area depicted in gray in Fig. 2, users denoted as u with traffic demand D_u are positioned uniformly at random. To achieve a uniform distribution on the sphere, the azimuth angles ϕ_u of the users are drawn from a uniform distribution

$$\phi_u \sim U(0, 2\pi), \tag{1}$$

where $U(a, b)$ represents the uniform distribution over the interval $[a, b]$. The elevation angles θ_u of the user positions are drawn from the adapted uniform distribution

$$\theta_u \sim \arccos(U(\cos(\theta_{\text{lim}}), 1)), \tag{2}$$

where $\theta_{\text{lim}} = \frac{r_{\text{footprint}}}{r_{\text{Earth}}}$ is the limiting angle of the spherical circle representing the satellite serving area. The transformation of the uniform distribution assures a uniform density of points around the poles, see the Appendix A for a derivation.

B. TIME-FREQUENCY RESOURCE GRID

The users are served on a share of physical resources in the K_a-band centered around the center frequency f_c. The time-frequency grid of the transmission resources is sketched in Fig. 3. The transmission band is separated into N_{subband} sub-bands and a transmission time corresponding to one beam hopping cycle of duration T_c is considered. The duration of the beam hopping cycle is smaller or equal than the coherence time of the channel that is below 100 ms [32, Table 7.2-1]. It is also assumed that the frequency-selective channel is constant within each sub-band, but varies from sub-band to sub-band, i.e., the sub-band bandwidth is equal to the coherence bandwidth of the channel. From this follows that one independent channel realization is sufficient to describe the channel fading in a sub-band.

The time-frequency resources are further divided into time slots of duration T_{slot}, which correspond to the switching cycle of the beams, i.e., the time necessary to turn a beam on or off. As in [33], [34], it is assumed that channel state information (CSI) is available at the satellite for the considered beam hopping cycle. This could be warranted through a time division duplexing scheme where CSI is collected during intermittent uplink transmissions. The expected round trip time of 50 ms in LEO satellite communications [3] would allow the acquisition of accurate CSI within the expected channel coherence time of less than 100 ms [32, Table 7.2-1].

In each beam hopping cycle, a beam hopping pattern $\mathbf{Q} \in \{0, 1\}^{N_{\text{beam}} \times N_{\text{slot}}}$ is applied that defines which beam is activated in which time slot. N_{slot} is the number of slots in a beam hopping cycle and N_{beam} is the number of beams the satellite can form simultaneously. The different algorithms to define the binary matrix of the beam hopping pattern $\mathbf{Q}$ are described in Section IV.

C. ANTENNA ARRAY

The satellite is equipped with a multi-panel antenna array, where each of the N_{beam} panels is connected to a radio frequency (RF) chain and generates one beam. The beams are steered to fixed positions on the ground, where the beam centers form a flat-topped hexagonal grid centered at the (0,0,0)-coordinate.

The antenna array is sketched in the lower right corner of Fig. 2 and consists of N_x panels in x'-direction and N_y panels in y'-direction. A rotated, re-centered, Cartesian coordinate system (x',y',z') is introduced that is centered at the corner of the antenna array. Each panel consists of $n_x \times n_y$ antenna elements in x' and y' directions with uniform antenna element spacing d_x in x'-direction and d_y in y'-direction

$$d_x = d_y = \frac{\lambda}{2}, \tag{3}$$

where $\lambda = \frac{c_0}{f_c}$ is the wavelength at frequency f_c with c_0 being the speed of light in vacuum. No additional spacing is added between the antenna panels. The total number of antenna elements for each beam is

$$N = n_x n_y. \tag{4}$$

The array steering vector $\mathbf{a}_u^{(b)} \in \mathbb{C}^{1\times N}$ of one panel at position (X, Y) used to transmit beam $b = Y\frac{N_x}{n_x} + X$ is [35, Sec. 6.10]

$$\mathbf{a}_u^{(b)} = \mathbf{a}_u^{(X)} \otimes \mathbf{a}_u^{(Y)}, \tag{5}$$

where $\otimes$ denotes the Kronecker product. Vectors $\mathbf{a}_u^{(X)}$ and $\mathbf{a}_u^{(Y)}$ are defined in Appendix B and denote the phase shift

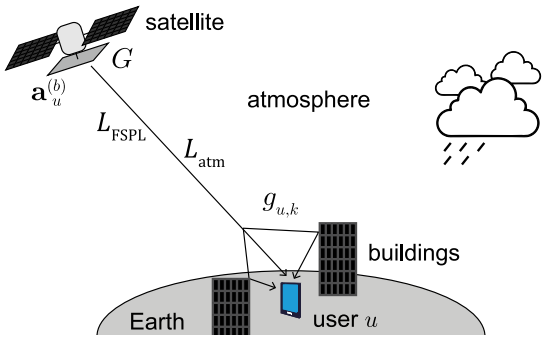

FIGURE 4. Sketch of the channel fading effects. The signal is affected by the array steering vector $\mathbf{a}_u^{(b)}$ of each beam b, the free space path loss L_{FSPL}, atmospheric losses L_{atm}, and Rician fading $g_{u,k}$ stemming from the multi-path propagation in the environment of the user.

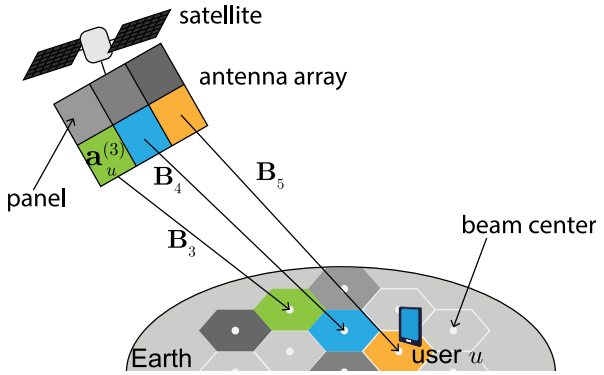

FIGURE 5. Illustration of beamforming scheme. Each panel of the antenna array is steered towards the cell center of a hexagonal grid by the analog precoder $\mathbf{B}_b$ that compensates the effect of the array steering vector $\mathbf{a}_u^{(b)}$ at the cell center.

vectors of a uniform linear array in x-direction and y-direction respectively.

D. CHANNEL MODEL

The channel fading is modeled as a combination of large scale fading and small scale fading. Figure 4 shows a sketch of the fading effects affecting the link between the satellite and the user.

1) LARGE SCALE FADING

The total path loss L_u that affects the link between user u and the satellite is modeled as

$$L_u = L_{\text{FSPL}}^{(u)} \cdot L_{\text{atm}}^{(u)}, \tag{6}$$

or, if expressed in dB,

$$L_u\big|_{\text{dB}} = L_{\text{FSPL}}^{(u)}\big|_{\text{dB}} + L_{\text{atm}}^{(u)}\big|_{\text{dB}}, \tag{7}$$

where $L_{\text{FSPL}}^{(u)}$ is the free space path loss (FSPL) depending on the distance between the user and the satellite and $L_{\text{atm}}^{(u)}$ describes the losses due to atmospheric effects, such as rain or cloud attenuation.

2) SMALL SCALE FADING

The line of sight (LOS)-link between user and satellite [36] is modeled as Rician fading according to [32, Table 7.2-1]. The Rician fading coefficients $g_{u,k} \in \mathbb{C}$ affecting the transmission of user u in sub-band k follow i.i.d. Rician distributions

$$g_{u,k} \sim \mathcal{N}(\mu, \sigma) + j\mathcal{N}(\mu, \sigma), \tag{8}$$

with $\mu = \sqrt{\frac{K}{2(K+1)}} \in \mathbb{R}$ and $\sigma = \sqrt{\frac{1}{2(K+1)}} \in \mathbb{R}$, where K is the Rician K-factor.

Note that $g_{u,k}$ is independent of the satellite beam b, because the propagation channel is identical for all beams from a satellite. Between the satellite and the user, the transmitted wave propagates through free space and only experiences multi-path propagation in the vicinity of the user. Therefore, the small scale fading depends only on the user environment and is identical for all beams [5], [15], [16]. This is a distinctive characteristic of satellite communications that leads to strong co-channel interference [5].

The co-channel interference leads to the Rician fading factor $g_{u,k}$ being constant across all beams received from the satellite for a single user in a sub-band. This consistency results in significant interference, which is mitigated through the use of a hybrid precoding scheme. It's important to note that the Rician fading factor only changes across sub-bands and between different users, but is constant over all beams in the same sub-band for a user.

The time-varying frequency response $\mathbf{H}_{u,k}^{(b)} \in \mathbb{C}^{1\times N}$ of the channel of beam b towards user u on sub-band k can be denoted as

$$\mathbf{H}_{u,k}^{(b)} = \sqrt{GL_u} g_{u,k} \mathbf{a}_u^{(b)}, \tag{9}$$

where $G \in \mathbb{R}$ is the maximum antenna gain of the antenna array, L_u is the large scale fading defined in (6), $g_{u,k}$ is the Rician fading coefficient from (8), and $\mathbf{a}_u^{(b)}$ is the array steering vector from (5).

The signal is also affected by a Doppler shift induced by the movement of the satellite and a signal delay due to the propagation time between the user and the satellite that induces a frequency shift in the frequency domain. It is assumed that these effects can be accurately estimated and compensated, as proposed in [6], [7]. Therefore, no Doppler shift is included in (9).

E. HEXAGONAL GRID ANALOG BEAMFORMING

The analog beamformer defines the beam direction and is chosen based on the beam centers of the fixed beam pattern illustrated in Fig. 5. The beams are arranged in a flat-topped hexagonal grid with a center beam at coordinate $(0, 0, 0)$ surrounded by rings of beams. The phase shifts of the analog precoder are defined such that they compensate the array steering vector at the center of the beam.

To define the analog beamforming matrix, let θ_b and ϕ_b denote the angles from the antenna array to the center of beam b. Then, the phase shifts of the analog precoder are

$$a_b^{(x,y)} = e^{-j\pi x \Phi_x^{(b)}} e^{-j\pi y \Phi_y^{(b)}}, \tag{10}$$

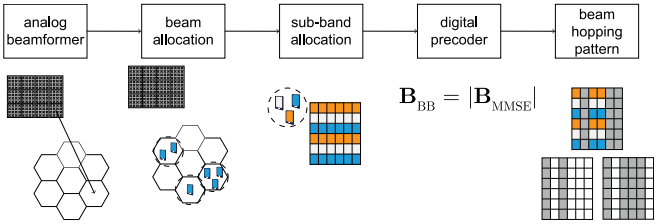

FIGURE 6. Block diagram of the system.

where we introduce $\Phi_x^{(b)} = \sin(\theta_b)\cos(\phi_b)$ and $\Phi_y^{(b)} = \sin(\theta_b)\sin(\phi_b)$ to shorten the notation and x and y are the indices of each antenna element. Note that this is the conjugate of the array steering vector at this position.

The antenna array is divided into panels with each panel being associated to one beam. The elements of each panel are steered by the analog precoder towards the center of a different beam. An example of the antenna array with panel-beam association is shown in Fig. 5.

In matrix form, the analog precoder $\mathbf{B}_b \in \mathbb{C}^{N\times 1}$ applied to the panel steering the beam b, can be denoted as

$$\mathbf{B}_b = \frac{1}{\sqrt{N}} \begin{bmatrix} e^{-j\pi(bn_x)\Phi_x^{(b)}} e^{-j\pi(bn_y)\Phi_y^{(b)}} \\ e^{-j\pi(1+bn_x)\Phi_x^{(b)}} e^{-j\pi(bn_y)\Phi_y^{(b)}} \\ \vdots \\ e^{-j\pi(n_x-1+bn_x)\Phi_x^{(b)}} e^{-j\pi(n_y-1+bn_y)\Phi_y^{(b)}} \end{bmatrix}, \quad (11)$$

where N is the number of antenna elements per panel. Each entry in (11) compensates the phase shifts of the array steering vector experienced at the beam center on the ground of the respective antenna element on the panel steered towards beam b.

The complete analog precoder describing the phase shift of all antenna elements in the antenna array can be denoted as a block diagonal matrix $\mathbf{B}_{\mathrm{RF}} \in \mathbb{C}^{N_{\mathrm{beam}}N\times N_{\mathrm{beam}}}$

$$\mathbf{B}_{\mathrm{RF}} = \begin{bmatrix} \mathbf{B}_0 & & \mathbf{0} \\ & \mathbf{B}_1 & \\ & \ddots & \\ \mathbf{0} & & \mathbf{B}_{N_{\mathrm{beam}}-1} \end{bmatrix}, \quad (12)$$

where $\mathbf{0}$ represents all zero elements of the appropriate size.

Figure 6 shows a block diagram of the system. In the first block, the analog beamformer is set to steer the antenna panels in the direction of the beam centers. This is sketched for one antenna panel that is pointed towards the center of one beam footprint.

F. RESOURCE ALLOCATION

1) BEAM SELECTION

After the generation of the beams by the analog beamformer, the users choose their serving beam. Each user is associated to the beam that offers the highest macroscopic receive power, i.e., the desired beam d_u for a given user u is chosen as

$$d_u = arg\,max_b \left| \mathbf{B}_b \sqrt{GL_u}\mathbf{a}_u^{(b)} \right|^2. \quad (13)$$

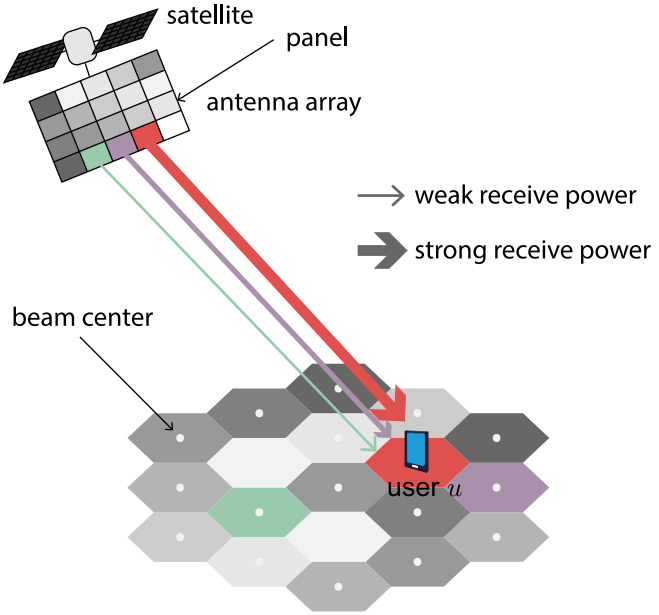

FIGURE 7. Sketch of the beam selection scheme. The thickness of the arrows indicates the strength of the received power from the array panels. The signals of three exemplary beams are sketched, the user connects to the beam with the strongest receive signal among all satellite beams.

The maximized expression is proportional to the macroscopic power received from beam b before digital precoding. The expression is the combination of the analog precoder of each beam, the array steering vector at the user position, the antenna gain, and the large scale fading experienced by the user. This beam association strategy assures that the signal from the interfering beams is weaker than the desired signal.

The process is illustrated for three exemplary beams in Fig. 7. The strength of the received signal is evaluated at the user for each beam. The user then chooses the strongest beam as its serving beam.

2) SUB-BAND ALLOCATION

Once the users are associated to a beam, the resources are distributed to the users by the sub-band allocation. For each beam, the users associated to this beam are assigned transmission resources in the form of sub-bands by a round-robin scheduler. An example of the sub-band allocation is given in the sub-band allocation part of Fig. 6. It shows the sub-band allocation for a beam serving three users. Each of the three users is assigned to a sub-band, the procedure is repeated until no more sub-bands are available.

As the focus of this work is the performance evaluation of beam hopping schemes, a well-known sub-band allocation scheme is chosen, whose effects on the system performance are well known. This makes the simulation results easier to interpret and assures that the observed effects can be related to the performance of the beam hopping schemes.[1]

[1]Proposed beam hopping methods can be combined with more sophisticated sub-band allocation methods, as discussed in Section VI.

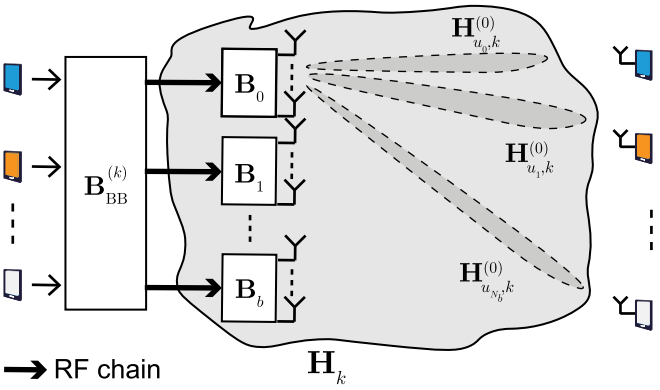

FIGURE 8. Signal processing chain with effective channel $\mathbf{H}_k$ of sub-band k.

G. DIGITAL PRECODING

To combat co-channel interference, the transmitter is equipped with a digital (or base-band) precoder [37]. A sketch of the signal processing chain is shown in Fig. 8. It shows the data transmission on sub-band k. The user data streams of the scheduled users are mapped to RF chains by the digital precoder $\mathbf{B}^{(k)}_{\mathrm{BB}} \in \mathbb{C}^{N_{\mathrm{beam}} \times N_{\mathrm{stream}}}$. N_{stream} is the number of streams transmitted per time slot and sub-band, which is equal to the number of beams as one user transmits per beam and sub-band ($N_{\mathrm{stream}} = N_{\mathrm{beam}}$). At the end of each RF chain, the analog precoder maps the transmit signal to the antenna elements.

As we want the simulation results to be reflective of the performance of the beam hopping schemes, we choose a precoder whose behavior has been extensively studied. We choose an MMSE precoder, as satellite links often suffer from poor channel quality, and the MMSE prevents the problem of noise enhancement. The use of MMSE precoding for satellite communication has been validated in [38]. The MMSE precoder $\mathbf{B}^{(k)}_{\mathrm{MMSE}}$ on sub-band k is defined as

$$\mathbf{B}^{(k)}_{\mathrm{MMSE}} = \left(\mathbf{H}^H_k \mathbf{H}_k + \sigma_n^2 \mathbf{I}_{N_{\mathrm{RF}}}\right)^{-1} \mathbf{H}^H_k, \tag{14}$$

where $\mathbf{H}_k \in \mathbb{C}^{N_{\mathrm{beam}} \times N_{\mathrm{beam}}}$ is the effective channel matrix that describes the channel between each transmit beam and the respective scheduled user, including the analog precoder sketched in dark gray in Fig. 8. The effective channel can be defined as

$$\mathbf{H}_k = \begin{bmatrix} \mathbf{H}^{(0)}_{u_0,k} & \mathbf{H}^{(1)}_{u_0,k} & \cdots & \mathbf{H}^{(N_b)}_{u_0,k} \\ \mathbf{H}^{(0)}_{u_1,k} & \mathbf{H}^{(1)}_{u_1,k} & \cdots & \mathbf{H}^{(N_b)}_{u_1,k} \\ \vdots & \vdots & & \vdots \\ \mathbf{H}^{(0)}_{u_{N_b},k} & \mathbf{H}^{(1)}_{u_{N_b},k} & \cdots & \mathbf{H}^{(N_b)}_{u_{N_b},k} \end{bmatrix} \mathbf{B}_{\mathrm{RF}}, \tag{15}$$

with u_b being the user scheduled on beam b on the considered sub-band k, $\mathbf{H}^{(b)}_{u,k}$ being the time-varying frequency response of the channel between user u and beam b on sub-band k as defined in (9), and $N_b = N_{\mathrm{beam}} - 1$.

The number of beams corresponds to the number of users that simultaneously receive data on the same sub-band as one user is scheduled on each beam. In an abuse of notation, N_{beam} here refers to the number of beams with users associated to them, instead of the total number of beams. For the calculation of the precoder, perfect instantaneous channel state information (iCSI) is assumed.

To obtain the digital base-band precoder, the MMSE precoder is normalized such that the transmit power constraint is enforced on each beam, i.e., the digital precoder $\mathbf{B}^{(b,k)}_{\mathrm{BB}} \in \mathbb{C}^{1 \times N_{\mathrm{beam}}}$ on sub-band k affecting the transmission on beam b is set to

$$\mathbf{B}^{(b,k)}_{\mathrm{BB}} = \frac{1}{\left\| \left(\mathbf{B}^{(k)}_{\mathrm{MMSE}}\right)_{(b,:)} \right\|_{\mathrm{F}}} \left(\mathbf{B}^{(k)}_{\mathrm{MMSE}}\right)_{(b,:)}, \tag{16}$$

where $(\mathbf{A})_{(m,:)}$ denotes the row vector in row m of matrix $\mathbf{A}$ and $\|\cdot\|_{\mathrm{F}}$ denotes the Frobenius norm defined as

$$\|\mathbf{A}\|_{\mathrm{F}} = \sqrt{\sum_{i=1}^{m} \sum_{j=1}^{n} \left|(\mathbf{A})_{(i,j)}\right|^2}, \tag{17}$$

for the $(m \times n)$-matrix $\mathbf{A}$ with $(\mathbf{A})_{(i,j)}$ being the element in row i and column j of matrix $\mathbf{A}$.

The full digital precoder $\mathbf{B}^{(k)}_{\mathrm{BB}} \in \mathbb{C}^{N_{\mathrm{beam}} \times N_{\mathrm{beam}}}$ is then

$$\mathbf{B}^{(k)}_{\mathrm{BB}} = \begin{bmatrix} \mathbf{B}^{(0,k)}_{\mathrm{BB}} \\ \mathbf{B}^{(1,k)}_{\mathrm{BB}} \\ \vdots \\ \mathbf{B}^{(N_b,k)}_{\mathrm{BB}} \end{bmatrix}. \tag{18}$$

H. USER RATE CALCULATION

1) RECEIVED SIGNAL

The signal $y_{u,k,s} \in \mathbb{C}$ received by user u on sub-band k in time slot s can be denoted as

$$y_{u,k,s} = \sum_{b \in \mathcal{B}} \sqrt{P_{\mathrm{tx}}} \mathbf{H}^{(b)}_{u,k} (\mathbf{Q})_{b,s} \mathbf{B}_b \mathbf{B}^{(b,k)}_{\mathrm{BB}} \mathbf{s}_k(t) + n_k, \tag{19}$$

where $\mathcal{B}$ is the set of all beam indices,[2] n_k is additive white Gaussian noise with noise power σ_n and $\mathbf{s}_k(t) \in \mathbb{C}^{N_{\mathrm{beam}} \times 1}$ is the vector of unit norm transmit symbols for each user scheduled on this sub-band in this time frame. P_{tx} denotes the constant transmit power allocated per sub-band. Further, the frequency selective channel response $\mathbf{H}^{(b)}_{u,k} \in \mathbb{C}^{1 \times N}$ is used as defined in (9), the beam hopping matrix $\mathbf{Q} \in \{0,1\}^{N_{\mathrm{beam}} \times N_{\mathrm{slot}}}$ is defined in Section II-B, the analog precoder $\mathbf{B}_b \in \mathbb{C}^{N \times 1}$ in (11), and the digital precoder $\mathbf{B}^{(b,k)}_{\mathrm{BB}} \in \mathbb{C}^{1 \times N_{\mathrm{beam}}}$ in (16).

The received signal can be split into the desired received signal, the interfering received signal from the other beams, and noise resulting in

$$y_{u,k,s} = \underbrace{\sqrt{P_{\mathrm{tx}}} \mathbf{H}^{(d_u)}_{u,k} (\mathbf{Q})_{d_u,s} \mathbf{B}_{d_u} \mathbf{B}^{(k)}_{\mathrm{BB}} \mathbf{s}_k(t)}_{\text{desired signal}} \tag{20}$$

[2] $\mathcal{B}$ could also be considered the set of beam indices that have users to serve and are thus active in the considered beam hopping cycle to reduce the calculation effort.

$$+ \underbrace{\sum_{i\in\mathcal{B}\setminus d_u} \sqrt{P_{\text{tx}}}\mathbf{H}_{u,k}^{(i)}(\mathbf{Q})_{i,s}\mathbf{B}_i\mathbf{B}_{\text{BB}}^{(k)}\mathbf{s}_k(t)}_{\text{interfering signal}} \tag{21}$$

$$+ \underbrace{n_k}_{\text{noise}}, \tag{22}$$

where d_u denotes the index of the beam serving user u.

2) SINR CALCULATION

The received power can be calculated by applying the Frobenius norm $\|\cdot\|_{\text{F}}$ to each of the terms defined above, leading to the receive power of the desired signal

$$r_d = (\mathbf{Q})_{d_u,s}P_{\text{tx}}\left\|\mathbf{H}_{u,k}^{(d_u)}\mathbf{B}_{d_u}\mathbf{B}_{\text{BB}}^{(k)}\right\|_{\text{F}}^2, \tag{23}$$

the received power of the interfering signals

$$r_i = \sum_{i\in\mathcal{B}\setminus d_u}(\mathbf{Q})_{i,s}P_{\text{tx}}\left\|\mathbf{H}_{u,k}^{(i)}\mathbf{B}_i\mathbf{B}_{\text{BB}}^{(k)}\right\|_{\text{F}}^2, \tag{24}$$

where $\mathcal{B}$ is the set of all beam indices, and the noise power

$$r_n = \sigma_n^2. \tag{25}$$

With this, we can define the SINR for the scheduled user u on sub-band k in time slot s as the ratio of desired received power and interference plus noise:

$$\text{SINR}_{u,k,s} = \frac{(\mathbf{Q})_{d_u,s}P_{\text{tx}}\left\|\mathbf{H}_{u,k}^{(d_u)}\mathbf{B}_{d_u}\mathbf{B}_{\text{BB}}^{(k)}\right\|_{\text{F}}^2}{\sum_{i\in\mathcal{B}\setminus d_u}(\mathbf{Q})_{i,s}P_{\text{tx}}\left\|\mathbf{H}_{u,k}^{(i)}\mathbf{B}_i\mathbf{B}_{\text{BB}}^{(k)}\right\|_{\text{F}}^2 + \sigma_n^2}. \tag{26}$$

3) SHANNON-HARTLEY RATE

With the user SINR in slot s in each sub-band k, we can calculate the user rate $R_u \in \mathbb{R}$ as

$$R_u = \sum_{s=0}^{N_{\text{slot}}-1}\sum_{k\in\mathcal{K}_u} BT_{\text{slot}}\log_2\left(1+\text{SINR}_{u,k,s}\right), \tag{27}$$

where $\mathcal{K}_u$ is the set of sub-bands allocated to user u, N_{slot} is the number of slots in a beam hopping cycle, B is the sub-band bandwidth, and T_{slot} is the duration of a slot. The rate R_u represents the number of bits transmitted in a beam hopping cycle.

I. POWER CONSUMPTION MODEL

In this section, we derive a power consumption model from different models in literature. Several power consumption models for hybrid combining receiver architectures are derived in [27]. As a starting point, we use the model for an architecture with variable phase shifters in subsets of antennas shown in [27, Fig. 2(b)] and described in [27, (9)].

The model from [27] is designed to describe the power consumption at the receiver and contains a term for low noise amplifiers at each antenna that are used for this purpose. As we are modeling the power consumption at the transmitter and low noise amplifiers are not present in the transmitter architecture, the low noise amplifier term N_rP_{LNA} in (9)[27] is not considered in this paper.

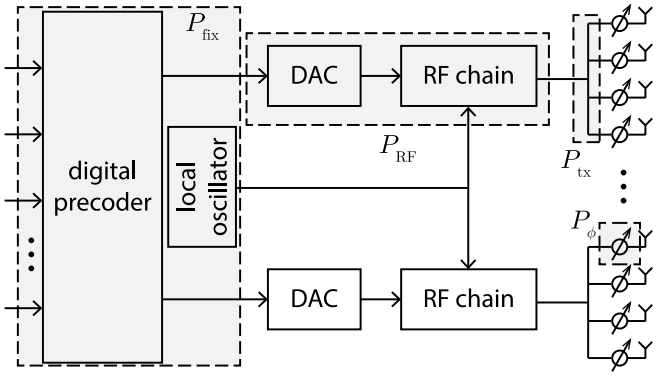

FIGURE 9. Block diagram of the components considered in the power consumption model.

The power consumption is thus composed of the power utilized by the phase shifters at each antenna element $P_\phi\ N_rP_{PS}$ in (9) [27], the power consumed in each RF chain P_{RF}, and a fixed term of power consumption P_{fix}. We include the power consumption of the digital analog converter (DAC) in the RF chain power consumption and combine P_{RFC} in (9) [27] and P_{ADC} in (9) [27] into P_{RF}, as it is difficult to find separate measurement results for the two effects in literature. The fixed power consumption P_{fix} contains the power consumed by the digital precoder, the local oscillator used for synchronization, as well as all other constant power consumption terms.

In addition to the power consumed by the hybrid architecture, the transmit power is the main contributing factor to the power consumption. It can be modeled as the transmit power P_{tx} divided by the efficiency of the power amplifier η [28, Ch. 15]. In our model the fixed power P_{fix} is always utilized, whereas the remaining power consumption depends on the beam activation pattern $\mathbf{Q}$. It is assumed that a deactivated beam does not consume any power. This implies that the sleep mode power consumption of the RF chain is included in the fixed power consumption term.

The proposed model for the total power consumption P in a beam hopping cycle is

$$P(\mathbf{Q}) = P_{\text{fix}} + \frac{1}{N_{\text{slot}}}\left\|\left(\frac{1}{\eta}P_{\text{tx}} + P_{\text{RF}} + N_bP_\phi\right)\mathbf{Q}\right\|_1, \tag{28}$$

where $\|\cdot\|_1$ denotes the L^1-norm, i.e., the sum of the absolute values of all matrix elements. A block diagram of the system is shown in Fig. 9, each power consumption term from (28) is mapped to a component it represents.

III. BEAM HOPPING OPTIMIZATION PROBLEM FORMULATION

This section defines the power minimization problem that has to be solved in order to find the optimal beam hopping pattern under which to operate the LEO satellite system.

The goal of the beam hopping pattern design is to minimize the power consumption while meeting the user

demands and respecting the system capabilities, i.e., the number of available beams and the frame duration. This can be formulated as the optimization problem

$$\mathbf{Q}_{\text{optimal}} = \underset{\mathbf{Q}\in\{0,1\}^{N_{\text{beam}}\times N_{\text{slot}}}}{\arg\min} \quad P(\mathbf{Q}) \qquad (29)$$
$$\text{s.t.} \quad R_u(\mathbf{Q}) \geq D_u \quad \forall u \in \mathcal{U},$$

where $\mathbf{Q}_{\text{optimal}} \in \{0,1\}^{N_{\text{beam}}\times N_{\text{slot}}}$ is the beam hopping pattern defined in Section II-B, $P(\mathbf{Q})$ is the power consumption in the frame defined in (28), R_u is the user rate defined in (27) with the dependence on the beam hopping pattern made explicit, and D_u is the user demand of user u. Since the user rate depends on the interference, which in turn depends on the beam hopping pattern $\mathbf{Q}$, this problem does not have a closed form solution. In the following, we present our proposed beam hopping solutions, along with benchmark methods.

IV. BEAM HOPPING ALGORITHMS

Five solution approaches are presented. An ILP formulation (Section IV-A) with interference estimation, which is an adaptation of the work in [10] to LEO satellite systems, is proposed and investigated in order to evaluate the applicability of GEO solutions in LEO systems. An interference-aware greedy heuristic algorithm (Section IV-B) is proposed to enhance the system's performance. Finally, three benchmark solutions that give bounds for the algorithm performance are defined.

The benchmarks include an exhaustive search (Section IV-C) that produces an optimal solution, a full illumination beam pattern (Section IV-E) that gives a reference on the performance if no beam hopping pattern is employed, and a random beam hopping pattern (Section IV-D) that shows how much the algorithms improve performance compared to random decisions.

A. PROPOSED GEO-ADAPTED BEAM HOPPING PATTERN

In (29), the value of the constraint depends on the optimization variable, i.e., the user rate depends on the beam hopping pattern, because the beam hopping pattern influences the interference power, which impacts the transmission rate. In [10], an interference estimation algorithm is employed to remove this dependency. The simplified problem can then be solved with well-established optimization techniques. The interference estimation algorithm is described in Section IV-A.1, the simplified optimization problem is solved in Section IV-A.2. A flow chart of the algorithm and exemplary algorithm outputs are shown in Fig. 10.

1) INTERFERENCE ESTIMATION

To find an average interference power, we consider $\mathcal{U}_b$, the set of users served by beam b. The beam demand $D_{\text{beam},b} \in \mathbb{R}$ of beam b is the sum of the user demands of the users associated to this beam

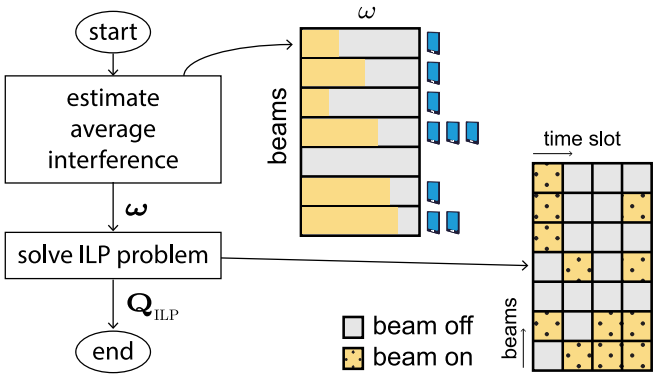

FIGURE 10. Flow Chart of proposed *adapted GEO* algorithm with exemplary illumination probability and beam hopping pattern.

$$D_{\text{beam},b} = \sum_{u\in\mathcal{U}_b} D_u. \qquad (30)$$

The achievable rate $R_{\text{beam},b} \in \mathbb{R}$ of beam b is the sum of the achievable rates of the users associated to this beam

$$R_{\text{beam},b} = \sum_{u\in\mathcal{U}_b} R_u. \qquad (31)$$

The individual beam rates can be stacked into the vector $\mathbf{R} \in \mathbb{R}^{N_{\text{beam}}}$.

To find an average interference power, we define an illumination probability $\omega_b \in [0,1]$ for beam b. Stacked in a vector, the beam illumination probabilities give the illumination probability vector $\boldsymbol{\omega} \in [0,1]^{N_{\text{beam}}}$. With this illumination probability, the SINR on sub-band k can be calculated as

$$\text{SINR}_{u,k}(\boldsymbol{\omega}) = \frac{P_{\text{tx}} \left\| \mathbf{H}_{u,k}^{(d_u)} \mathbf{B}_{d_u} \mathbf{B}_{\text{BB}}^{(k)} \right\|_{\text{F}}^2}{\sum_{i\in\mathcal{B}\setminus d_u} \omega_b P_{\text{tx}} \left\| \mathbf{H}_{u,k}^{(i)} \mathbf{B}_i \mathbf{B}_{\text{BB}}^{(k)} \right\|_{\text{F}}^2 + \sigma_n^2}, \qquad (32)$$

where d_u is the index of the beam serving user u. Note that the illumination probability only affects the interfering links in this expression. The desired link is considered to be on, when the beam is transmitting. The only difference to the calculation of the SINR affecting the transmission in (26) is the absence of the beam hopping pattern $\mathbf{Q}$ that is replaced with the illumination probability $\boldsymbol{\omega}$.

The illumination probability is determined in an iterative process that starts with zero illumination probability on all beams and increases the illumination probability to meet the user demands depending on the interference according to the illumination probability. The illumination probability increases in each step until it converges to the final illumination probability that represents the duration a beam needs to be illuminated to serve the demands of all of its users while considering the interference of the other beams. The algorithm is stated in Algorithm 1 in which $\mathbf{0}_m$ represents the all zero column vector of length m and $\boldsymbol{\infty}_m$, the vector of length m with all infinity elements.

The termination threshold ε_c assures that the algorithm stops after the illumination probabilities do not significantly

Algorithm 1 Average Interference Estimation

Initialize: $\boldsymbol{\omega} = \mathbf{0}_{N_{\text{beam}}}$, $\mathbf{R} = \mathbf{0}_{N_{\text{beam}}}$, $\mathbf{R}' = \infty_{N_{\text{beam}}}$
while $||\mathbf{R} - \mathbf{R}'||_{\text{F}} > \varepsilon_c$ **do**
  $\mathbf{R}' \leftarrow \mathbf{R}$
  for all $b \in \mathcal{B}$ **do**
    $(\mathbf{R})_{(b)} \leftarrow R_b(\text{SINR}_{u,k}(\boldsymbol{\omega}))$
    $(\boldsymbol{\omega})_{(b)} = \min\left(1, \frac{D_b}{(\mathbf{R})_{(b)}}\right)$
  end for
end while
return $\boldsymbol{\omega}$

change in an iteration. The threshold is chosen to be larger than zero in order to avoid infinite loops in case of numerical inaccuracies.

2) SIMPLIFIED OPTIMIZATION PROBLEM

The new formulation of the simpler optimization problem with the fixed illumination probabilities $\boldsymbol{\omega}$ is

$$\mathbf{Q}_{\text{ILP}} = \underset{\mathbf{Q}\in\{0,1\}^{N_{\text{beam}}\times N_{\text{slot}}}}{\arg\min} \quad P(\mathbf{Q}) \tag{33}$$

$$\text{s.t.} \quad R_u(\mathbf{Q}, \boldsymbol{\omega}) \geq D_u \quad \forall u \in \mathcal{U}, \tag{34}$$

where the user rate R_u is calculated with the constant user slot rate $R_{\text{s},u}$ defined as

$$R_{\text{s},u} = \sum_{k\in\mathcal{K}_u} BT_{\text{slot}} \log_2\left(1 + \text{SINR}_{u,k}(\boldsymbol{\omega})\right) \tag{35}$$

to be

$$R_u(\mathbf{Q}, \boldsymbol{\omega}) = R_{\text{s},u} \sum_{s=0}^{N_{\text{slot}}-1} (\mathbf{Q})_{d_u,s}. \tag{36}$$

Here, the slot rate of a user is considered to be constant, making the constraint linear. Hence, the optimization constraint only has to verify that a minimum amount of slots is illuminated in order to match the user demand.

This results in an ILP problem, which can be solved using one of many available solvers, we choose the Python-MIP solver [39].

In the following, the proposed GEO-adapted beam hopping approach will be referred to as proposed *adapted GEO* method.

B. PROPOSED INTERFERENCE-AWARE GREEDY BEAM HOPPING PATTERN

The interference estimation from Section IV-A1 is not suited for a LEO communication system as will be seen in Section V-C. However, the iterative approach can be used to set the beam hopping pattern with a greedy algorithm, as illustrated in Fig. 11. The proposed algorithm is described in Algorithm 2, where $\mathbf{1}_{M\times N}$ denotes the $(M \times N)$-matrix with all one elements and $\mathbf{0}_{M\times N}$ the $(M \times N)$-matrix with all zero elements. The idea of the algorithm is to illuminate each beam until the user demand can be met while only considering the beams illuminated so far as interference.

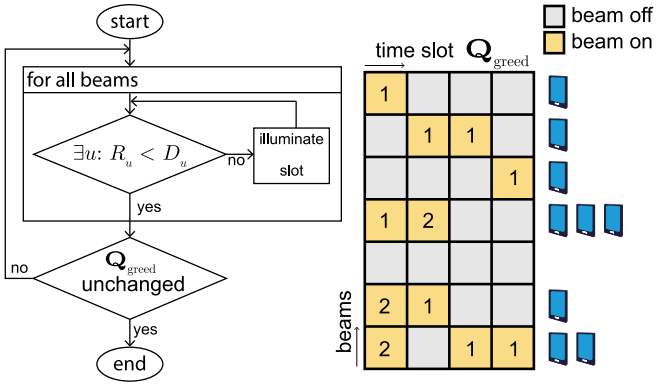

FIGURE 11. Flow chart of the proposed *greedy* algorithm with an exemplary illumination pattern. The slots marked with a 1 are illuminated in the first iteration of the algorithm, the slots marked with a 2 are illuminated in the second iteration after adjustment for the interference from the other beams. The number of users next to each beam indicate the traffic load on the beam.

Algorithm 2 Proposed Greedy Interference-Aware Method

Initialize: $\mathbf{Q}_{\text{greed}} = \mathbf{0}_{N_{\text{beam}}\times N_{\text{slot}}}$, $\mathbf{Q}'_{\text{greed}} = \mathbf{1}_{N_{\text{beam}}\times N_{\text{slot}}}$
while $\mathbf{Q}_{\text{greed}} \neq \mathbf{Q}'_{\text{greed}}$ **do**
  $\mathbf{Q}'_{\text{greed}} \leftarrow \mathbf{Q}_{\text{greed}}$
  for all $b \in \mathcal{B}$ **do**
    if $\sum_{t=0}^{n_{\text{slot}}} (\mathbf{Q}_{\text{greed}})_{(b,t)} < N_{\text{slot}}$ **then**
      for all $u \in \mathcal{U}_b$ **do**
        calculate $R_u(\mathbf{Q}_{\text{greed}})$ according to (27)
      end for
      if $\exists u \in \mathcal{U}_b$: $R_u < D_u$ **then**
        $i_{\text{slot}} = arg\,min_{s\in\mathcal{S}} \sum_{s\in\mathcal{S}} \sum_{i\in\mathcal{B}\setminus b} (\mathbf{Q}_{\text{greed}})_{(i,s)}$
        $(\mathbf{Q}_{\text{greed}})_{(b,i_{\text{slot}})} \leftarrow 1$
      end if
    end if
  end for
end while
return $\mathbf{Q}_{\text{greed}}$

Algorithm 2 starts with an initialization of the beam hopping matrix $\mathbf{Q}_{\text{greed}}$ to zeros, i.e., all beams are deactivated. $\mathbf{Q}'_{\text{greed}}$ is initialized to a value different to $\mathbf{Q}_{\text{greed}}$ to assure that the algorithm does not abort the calculation in the initial state. After saving the state of $\mathbf{Q}_{\text{greed}}$ in the previous iteration, the algorithm loops over all satellite beams.

For each beam, the user rates depending on the current beam hopping matrix are calculated for the users in the set $\mathcal{U}_b$ that is composed of all users associated to beam b. If any user's rate is lower than its demand, the slot with the lowest number of active interferers out of the set of non-illuminated slots $\mathcal{S}$ is determined in Algorithm 10 and illuminated. The user rates are re-calculated until all user demands are met, or all slots are illuminated.

Proposition 1: Algorithm 2 converges after a finite number of iterations.

Proof: In each iteration the algorithm either illuminates at least one beam in one slot or is terminated, as the

Algorithm 3 Exhaustive Search

Initialize: $P_{\text{opt}} = \infty$, $P_{\text{subopt}} = \infty$, $\mathbf{Q}_{\text{opt}} = \mathbf{0}_{N_{\text{beam}} \times N_{\text{slot}}}$, $N_{\text{served}} = 0$, `sol_found` = *false*
for all $\mathbf{Q} \in \mathcal{Q}$ **do**
  calculate $P(\mathbf{Q})$ according to (28)
  calculate R_u $\forall u \in \mathcal{U}$ according to (27)
  if $R_u \geq D_u$ $\forall u$ **and** $P(\mathbf{Q}) < P_{\text{opt}}$ **then**
    $P_{\text{opt}} \leftarrow P(\mathbf{Q})$, $\mathbf{Q}_{\text{opt}} \leftarrow \mathbf{Q}$, $N_{\text{served}} \leftarrow N_u$, `sol_found` $\leftarrow$ *true*
  else if `sol_found` = *false* **then**
    calculate N'_{served} according to (41)
    if $N'_{\text{served}} > N_{\text{served}}$ **then**
      $P_{\text{subopt}} = P(\mathbf{Q})$, $\mathbf{Q}_{\text{opt}} = \mathbf{Q}$, $N_{\text{served}} = N'_{\text{served}}$
    else if $N'_{\text{served}} = N_{\text{served}}$ **and** $P(\mathbf{Q}) < P_{\text{subopt}}$ **then**
      $P_{\text{subopt}} \leftarrow P(\mathbf{Q})$, $\mathbf{Q}_{\text{opt}} \leftarrow \mathbf{Q}$
    end if
  end if
end for
return $\mathbf{Q}_{\text{opt}}$, `sol_found`

Algorithm 4 Random Beam Hopping Pattern

for $b \in \mathcal{B}$ **do**
  for $i \in [1, \ldots, N_{\text{slot}}]$ **do**
    $(\mathbf{Q}_{\text{rand}})_{(b,i)} \sim \mathrm{B}(p_{\text{ill}})$
  end for
end for
for $b \in \mathcal{B}$ **do**
  if $\|(\mathbf{Q}_{\text{rand}})_{(b,:)}\|_1 = 0$ **then**
    $(\mathbf{Q}_{\text{rand}})_{(b,N_{\text{slot}})} \leftarrow 1$
  end if
end for
return $\mathbf{Q}_{\text{rand}}$

Algorithm 5 Full Illumination Beam Hopping Algorithm

$\mathbf{Q}_{\text{all}} \leftarrow \mathbf{1}_{N_{\text{beam}} \times N_{\text{slot}}}$
return $\mathbf{Q}_{\text{all}}$

termination condition is fulfilled. Therefore the number of illuminated slots increases monotonically with each iteration. The number of illuminated slots is also upper bounded by the total number of slots and beams. Therefore, the algorithm must converge towards its solution after at most $N_{\text{beam}}N_{\text{slot}}$ iterations, which is a finite number. ■

In the following, this proposed interference-aware greedy heuristic beam hopping scheme will be referred to as the proposed *greedy* method.

C. EXHAUSTIVE SEARCH BEAM HOPPING PATTERN BENCHMARK

Since the optimization variable is an integer variable, it is possible to find the optimal solution $\mathbf{Q}_{\text{opt}}$ to the optimization problem in (29) through an exhaustive search over the space of distinct possible solutions $\mathcal{Q}$. The exhaustive search algorithm is stated in Algorithm 3.

It is possible to run into optimization problems that do not have a valid solution that does not violate the side constraint. For these cases, where it is not possible to meet the demand of all users, the solution that offers the lowest user outage is chosen as solution in Algorithm 7. If there are several solutions with the same lowest user outage, then the solution with the lowest power consumption is chosen from these solutions. This means that this exhaustive search algorithm drops users if their demand cannot be fulfilled. The alternative approach would be to maximize the throughput of these users. This approach is not chosen here as it contradicts the goal of minimizing the power consumption.

To reduce complexity, the implementation of the algorithm takes into account that, since the channel is constant over the beam hopping cycle, several optimal solutions will exist that are column permutations of $\mathbf{Q}_{\text{opt}}$. Solutions that are column permutations are not explored in order to reduce the calculation time. The set of distinct solutions is denoted by $\mathcal{Q}$. To further reduce computational complexity, the user rate is calculated and saved for all possible slot illumination patterns.

The optimal exhaustive search benchmark beam hopping algorithm will be referred to as *optimal* benchmark in the remainder of this paper.

D. RANDOM BEAM HOPPING PATTERN BENCHMARK

The random beam hopping pattern $\mathbf{Q}_{\text{rand}}$ serves as a reference to evaluate whether the decisions taken by the beam hopping pattern algorithm offer improvement over random decisions. In this algorithm, each beam is illuminated with a probability p_{ill} in each time slot according to a Bernoulli distribution $\mathrm{B}(p_{\text{ill}})$.

The algorithm to obtain the random beam hopping pattern $\mathbf{Q}_{\text{rand}}$ is stated in Algorithm 4. To assure that all beams with users to serve are illuminated at least once per beam hopping cycle, the last time slot of a beam is illuminated if the beam is deactivated in all time slots (in Algorithm 8 of Algorithm 4). This will slightly increase the interference in the last time slot, but for a sufficiently large amount of time slots in a beam hopping cycle, it is unlikely that this mechanism is activated and for low numbers of time slots, it assures that the users on each beam get a chance to receive data.

In the following the random beam hopping benchmark will be referred to as *random* benchmark.

E. FULL ILLUMINATION BEAM HOPPING PATTERN BENCHMARK

The full illumination beam hopping pattern $\mathbf{Q}_{\text{all}}$ serves as a reference for how much the power consumption can be reduced if beams are deactivated. The full illumination beam hopping scheme is defined in Algorithm 5, it activates all beams that serve users in all slots.

The full illumination benchmark beam hopping scheme will be referred to as *full illumination* benchmark in the following.

TABLE 1. Number of satellite positions and network realizations.

ε	positions	repetitions	scenario realizations
$90° \pm 0.5°$	138	15	2070
$55° \pm 0.5°$	194	11	2134
$25° \pm 0.5°$	499	5	2495

V. NUMERICAL EVALUATION OF BEAM HOPPING PATTERN PERFORMANCE

This section presents the results of the Monte Carlo simulations performed in order to compare the performance of the beam hopping algorithms presented in Section IV. First, the simulation setup and parameters are explained, then the beam hopping algorithms are compared in terms of computation time, power consumption, outage, and sum rate. The co-channel interference experienced by the users is analyzed in Section V-C.

A. SIMULATION SCENARIO

1) MONTE CARLO REALIZATIONS

To obtain a statistically relevant number of results, a large number of scenario realizations is simulated. The satellite position for each scenario realization is taken from a circular trajectory around the Earth at elevation angles $90°\pm0.5°$, $55°\pm0.5°$, and $25°\pm0.5°$ observed from the center of the satellite serving area. These positions are repeated in order to obtain results from at least 2000 realizations. For each realization, new random user positions are generated and independent Rician fading realizations are generated for each user. The macroscopic fading is calculated according to the user positions. The number of satellite positions and repetitions are shown in Table 1. The table shows the number of positions at each elevation angle ε, the number of realizations with this position and the total number of scenario realizations at each angle.

The user demand is set to a constant demand for all users. A demand of 10 Mbit/s corresponds to 100 kbit of data to transmit for this user in the 10 ms beam hopping cycle that is simulated.

2) SYSTEM PARAMETERS

The system parameters are chosen to match the 3rd Generation Partnership Project (3GPP) D1 scenario in [40]. The 3GPP D1 describes a regenerative satellite with steerable beams, i.e., a satellite with on-board processing capabilities that serves a fixed region on the ground. A similar system setup is used in [9] to evaluate the link quality in the satellite serving area.

The system parameters are shown in Table 2. Some parameters do not match the 3GPP reference scenario, they are marked with an asterisk. The antenna gain is set according to the link budget analysis in [9], the reference scenario value is 38.5 dBi.

The Rician K-factor is set depending on the satellite elevation angle ε according to the values for μ and σ provided in [32, 6.7.2-3b].

TABLE 2. System parameters.

Carrier	
carrier frequency f_c	30 GHz
sub-band bandwidth B	25 MHz
N_{subband}	10 (*)
Satellite	
altitude h_{sat}	600 km (LEO)
antenna gain G	60.5 dBi (*)
speed v_{sat}	7.56 km/s
Beam	
satellite beam radius r_{beam}	20 km (*)
transmit power P_{tx}	63 W
User	
speed	0 m/s (*)
Rician μ {35°, 55°, 90°}	{12.48, 5.97, 3.81}
Rician σ {35°, 55°, 90°}	{14.23, 9.47, 4.25}
antenna	omnidirectional
antenna gain G_u	0 dBi
receiver noise figure F	7 dB
user equipment temperature T_K	300°K

(*) not set according to 3GPP D1 reference scenario

The number of sub-bands is not defined in the reference scenario, it is set to 10 sub-bands to limit complexity while representing frequency-selective fading and allowing some flexibility in resource scheduling, the specification for the system bandwidth B is that it should be smaller than 1 GHz for carrier frequencies above 6 GHz. It is assumed that the full bandwidth can be used for data transmission, i.e., no guard band is included in this bandwidth.

The sub-band bandwidth is smaller than the minimum coherence bandwidth B_{coh} that can be calculated according to [32, Sec. 7.3.5.1.1] as

$$B_{\text{coh}} = \frac{1}{\alpha \tau_s}, \tag{37}$$

with α being a constant between 1 and 50 and τ_s being the delay spread. The delay spread is given as 10 ns in [32, Table 7.3.5.1.1-3] for LEO satellites operating in the K_a-band. The minimum coherence bandwidth is between 2 MHz in the worst cases and 100 MHz in the best cases. The worst cases should be assumed for the transmission of reference signals. Since we consider the transmission of data, it can be assumed that the channel is constant within the sub-band bandwidth of 25 MHz.

The atmospheric loss is calculated with the Python implementation from [41] according to ITU recommendations assuming that the footprint center coordinate is positioned at the coordinates specified in Table 3. These coordinates correspond to a position in central Tokyo, Japan. The model parameters used for the calculation of the atmospheric losses are listed in Table 3.

The noise power is calculated as

$$\sigma_n^2\big|_{\text{dBW}} = 10\log_{10}(k_B T_K B F) \approx -122 \text{ dBW}, \tag{38}$$

TABLE 3. Atmospheric loss model parameters.

Parameter	Value
latitude $(0, 0, 0)$-coordinate	35.67619190°
longitude $(0, 0, 0)$-coordinate	139.65031060°
diameter of receive antenna	0
unavailability	1%

TABLE 4. Time parameters.

Parameter	Symbol	Value
beam hopping cycle	T_c	10 ms
slot duration	T_{slot}	1 ms (*)

(*) increased to 2.5 ms for seven beam simulations

TABLE 5. Antenna array parameters.

Antenna Panel	
antennas	32×32
antenna spacing	$\lambda/2$
Panel Configuration	
19 beams	5×4
7 beams	4×2

where T_K is the user equipment temperature in Kelvin from Table 2, and k_B is the Boltzmann constant.

3) TIME PARAMETERS

The time structure is shown in Fig. 3, the frame duration is equal to or smaller than the coherence time of the channel T_c. The frame is divided into slots of duration T_{slot}, in which beams can be activated or deactivated. The time parameters are shown in Table 4.

A coherence time of less than 100 ms is expected for the satellite channel [32, Table 7.2-1]. The chosen time frame duration is well below the expected coherence time and could be increased in future work.

The slot duration is set to 1 ms to match the slot duration in 3GPP systems. In simulations where the *optimal* benchmark algorithm is employed, the slot duration is increased in order to reduce the search space of the exhaustive search algorithm and keep the simulation time feasible.

4) ANTENNA ARRAY PARAMETERS

The antenna array parameters are collected in Table 5. The setup is described in more detail in [9, Sec. II.A2]. The panel configuration defines the number of antenna array panels in x-direction and in y-direction.

5) POWER CONSUMPTION MODEL PARAMETERS

The parameters for the power consumption model shown in Table 6 are taken from recent literature. The additional comments in the references indicate the variable names in the referenced articles. The value for the power consumption of the RF chain P_{RF} is taken from [29], where a value for the transceiver chain power consumption is given. The fixed power consumption P_{fix} of the base-band processing and local oscillator is also taken from [29], where a value for the passive power consumption of the system is given. The power consumption of the phase shifters P_{PS} is taken from [30] for phase shifters with 3-bit resolution, which can closely approximate the performance of continuous phase shifters [42], [43]. The efficiency of the power amplifier η is chosen higher than most reference in literature, because we assume that a high quality amplifier is used at the upper bound of its operation region, where maximum efficiency is achieved. The high transmit power that is employed justifies this assumption, because amplifiers can operate more efficiently in the high power regime.

TABLE 6. Power consumption model parameters.

Parameter	Value	Reference
P_{fix}	100 mW	[29, Table I - μ]
P_{RF}	20 mW	[29, Table I - $\mathcal{D}_0$]
P_{PS}	16 mW	[30, Table II - $P_{\text{Ps}}(3)$]
η	0.7	[28, Section 15.8]

TABLE 7. Algorithm parameters.

Parameter	Value
ε_c	10^{-5}
p_{ill}	0.5

6) OPTIMIZATION ALGORITHM HYPER-PARAMETERS

The hyper-parameters of the optimization algorithms are collected in Table 7. The parameter ε_c for the interference estimation of the proposed *adapted GEO* algorithm assures that the interference estimation algorithm terminates even in the case of numerical errors that result in R and R' taking on slightly different values. It is thus set to a small value of $\varepsilon_c = 10^{-5}$. Smaller values showed equivalent results, larger values showed equivalent results until values of $\varepsilon_c > 1$. The simulation time is not significantly affected by changes in the values of ε_c.

The illumination probability p_{ill} of the random beam hopping scheme sets the percentage of illuminated beams. A probability of 0.5 is chosen to achieve maximum entropy, i.e., maximal randomness. Lower illumination probabilities lead to lower power consumption and higher outage, whereas a higher illumination probability leads to results that match the *full illumination* benchmark results, as more beams are activated with higher illumination probability.

7) OUTAGE DEFINITION

The user outage considered by the *optimal* benchmark scheme in Section IV-C and plotted in Fig. 12b, 13b, 15b, 16b and 17b is calculated as the percentage of users whose rate is lower than their requested demand in a beam hopping cycle, i.e., the outage is the fraction of users for which

$$R_u < D_u. \tag{39}$$

TABLE 8. Seven beam simulation parameters.

Parameter	Value
number of beams	7
N_u	10
T_{slot}	2.5 ms
D_u	{10, 100} Mbit/s

This can be formulated as

$$\text{outage} = 1 - \frac{N_{\text{served}}}{N_u}, \tag{40}$$

where N_u is the number of users in the satellite serving area and

$$N_{\text{served}} = \sum_{u \in \mathcal{U}} \begin{cases} 1, & R_u >= D_u \\ 0, & \text{else}, \end{cases} \tag{41}$$

with $\mathcal{U} = [0, N_u - 1]$ being the set of user indices.

This means that a user is assumed to be in outage if its demand is not fulfilled within a beam hopping cycle, which corresponds to a 10 ms time frame in our case. In practical systems, a less stringent requirement could be considered. For example, the considered time window to serve a user's demand could be increased, allowing higher latency in the transmission.

B. PERFORMANCE RESULTS FOR SEVEN BEAM SCENARIO

1) SIMULATION PARAMETERS

Given the prohibitive computational complexity of the *optimal* benchmark scheme, shown in Section V-E.2, a small scenario is considered first to compare the performance of the proposed algorithms against the *optimal* benchmark. The simulation parameters for the seven beam scenario are shown in Table 8. The number of beams is reduced, as well as the number of time slots in the beam hopping pattern. These parameter changes reduce the search space of the exhaustive search for the beam hopping pattern to $2^{2 \cdot 4} = 256$ possibilities. The number of users is reduced to 10 users, resulting in an average of 1.4 users per beam. A low demand and a high demand scenario are considered with user demands of 10 Mbit/s and 100 Mbit/s respectively.

2) LOW USER DEMAND

The seven beam simulation results for the low demand scenario are shown in Fig. 12. Figure 12a shows the power consumption of the beam hopping algorithms presented in Section IV for three different elevation angles: 90°, 55°, and 25°. The *full illumination* benchmark scheme gives an upper bound on the power consumption of the system. Comparison with the other beam hopping schemes shows that, for low user demand, the power consumption can be reduced by 75%. This shows the benefit of employing beam hopping schemes. The power consumption is halved with the *random* benchmark scheme that only activates 50% of the beams.

The power consumption slightly decreases at the lowest elevation angle for the *full illumination* benchmark scheme.

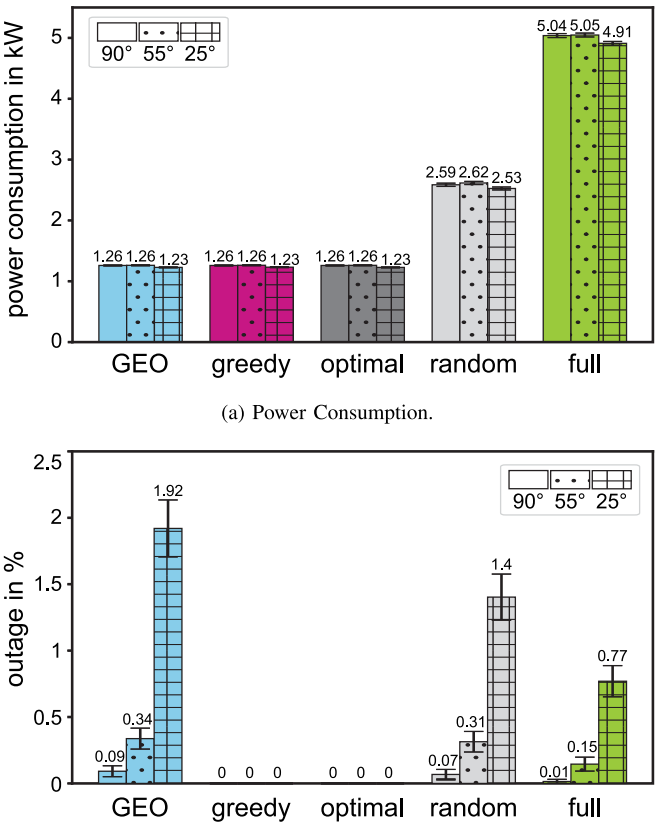

(a) Power Consumption.

(b) Outage.

FIGURE 12. Performance result for seven beam configuration with a user demand of 10 Mbit/s with 95% confidence interval. The proposed *greedy* scheme performs close to the *optimal* benchmark and can be used as near-optimal result in larger simulations.

This contradicts the intuition that more power is required to overcome the increased distance between the satellite and the serving area. This behavior is likely due to the distortion of the beam footprint on the ground at lower elevation angles that increases the cell sizes for some cells and reduces the cell size of other beams as is shown in [9]. The uneven cell sizes, result in a lower number of active beams, because the smaller cells are more likely to be empty. On average, 5.5 beams have users to serve at 90° elevation angle, whereas only 5.36 beams are active at 25° elevation angle.

The performance in terms of power consumption in Fig. 12a of the proposed *greedy* and the proposed *adapted GEO* scheme matches the performance of the *optimal* benchmark algorithm.

The outage of the different schemes is shown in Fig. 12b for the low demand scenario. The *full illumination* benchmark scheme performs close to the *optimal* benchmark for high elevation angles, but shows higher outage at 25° elevation angle. This shows that, in the low demand scenario, the user demand can be served without a sophisticated optimization algorithm because there are enough network resources to meet the demand. The outage of the *random* benchmark scheme is significantly higher, but the power

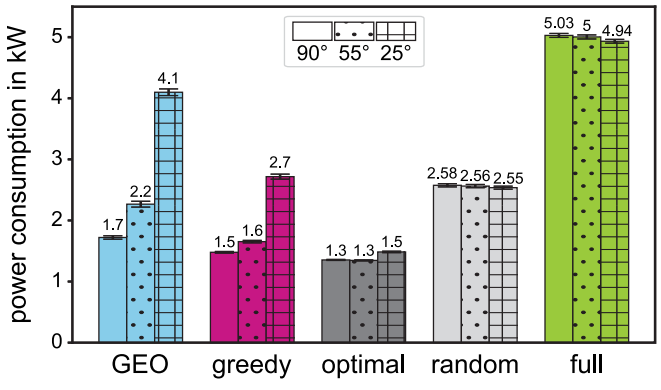

(a) Power Consumption.

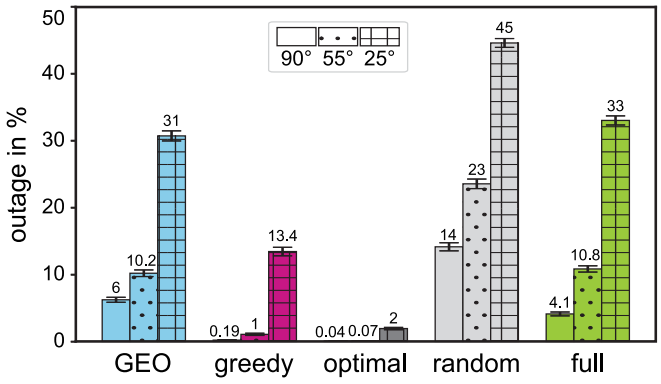

(b) Outage.

FIGURE 13. Performance result for seven beam configuration with a user demand of 100 Mbit/s with 95% confidence interval. At high network utilization, the proposed *greedy* performs closest to the *optimal* benchmark solution.

consumption is halved compared to the *full illumination* benchmark scheme. When the power consumption of the random scheme is further reduced to match the power consumption of the *optimal* benchmark solution, the outage is further increased.

The proposed *adapted GEO* beam hopping algorithm shows the highest outages of all schemes. The scheme is designed for GEO systems that operate at an elevation of 90°, which explains the poor performance at lower elevation angles. The proposed *adapted GEO* scheme is not suitable for use at low elevation angles. At high elevation angle, it can be used to lower the power consumption at the cost of slightly increased user outages.

The proposed *greedy* beam hopping algorithm can match the *optimal* benchmark solution in low demand scenarios.

3) HIGH USER DEMAND

The results of the seven beam high demand scenario are shown in Fig. 13. The power consumption of each scheme is shown in Fig. 13a. Compared to the low demand scenario, the power consumption is increased. The higher power consumption shows that the network is under higher load with the larger user rate demand. The power consumption of the proposed *greedy* scheme is closest to the *optimal* benchmark solution. In combination with the user outage results shown in Fig. 13b, the performance under high network load can be analyzed.

The proposed *greedy* scheme performs closest to optimal of the compared schemes. The optimal outage rate is almost achieved at the cost of higher power consumption. The trend of decreasing power consumption with decreasing elevation angles is inverted and the power consumption rises with falling elevation angle. This indicates that the schemes struggle to handle the high network load.

At 25° elevation angle, the power consumption of the *optimal* benchmark scheme is much lower than the power consumption of the proposed *greedy* scheme. The reason for the high power consumption of the proposed *greedy* scheme can be found in the handling of user demand that exceeds the network capacity. The *optimal* benchmark scheme does not serve users whose demand cannot be met, the proposed *greedy* scheme, on the other hand, offers as many resources as possible to high demand users.

The proposed *adapted GEO* scheme achieves the same outage rates as the full illumination scheme, but can reduce the power consumption of the system. The proposed *adapted GEO* scheme defaults to full illumination when the optimization problem has no solution, resulting in high power consumption in the case of overloaded networks.

In the high demand scenario at 25° elevation angle, the *random* benchmark scheme shows the lowest power consumption of the sub-optimal schemes, but leads to significantly higher outage rate. The achieved outage rates up to 45% are not suitable for network operation for any of the schemes, except the optimal scheme, whose outage is 2%.

The performance comparison with the *optimal* benchmark solution shows that the proposed *greedy* scheme performs close to optimal except in cases where the optimization problem has no solution. In these cases, the proposed *greedy* scheme tries to serve the users, whereas the *optimal* benchmark scheme drops users that cannot be satisfied. The proposed *adapted GEO* scheme fails to keep outages low. The *random* benchmark scheme performs poorly in all cases, but guarantees consistent power consumption, and the *full illumination* benchmark scheme has high power consumption and high outage. The proposed *greedy* beam hopping algorithm performs close to the *optimal* benchmark results, which allows us to consider it as near-optimal.

C. INTERFERENCE ESTIMATION

This section analyzes the performance of the interference estimation scheme described in Section IV-A1. The results in this section are necessary to explain the performance results in the following section.

To evaluate the interference estimation algorithm, we look at the interference power ECDF for the different schemes for different elevation angles in Fig. 14. The results are shown for the 19 beam system with 25 users with a 10 Mbit/s demand each.

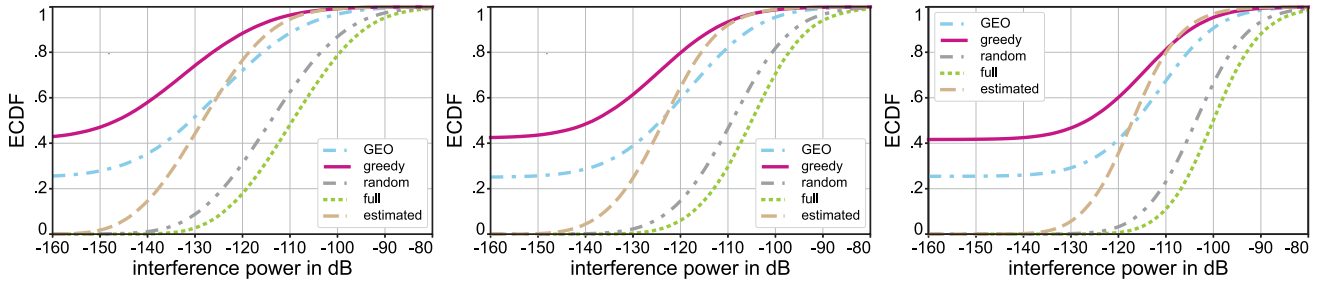

FIGURE 14. Comparison of estimated and actual system interference power ECDFs at different elevation angles for the 19 beam system with 25 users with 10 Mbit/s demand. The estimated interference does not match the interference in the proposed *adapted GEO* system.

The proposed *greedy*, *random* benchmark, and *full illumination* benchmark schemes do not use the interference estimation algorithm and their results are not influenced by its performance. Their interference is plotted for comparison and to gain a better understanding of the system behavior. The estimated interference power - plotted in dashed brown - does not match the actual interference power present in the proposed *adapted GEO* system plotted in dot-dashed blue.

The estimated interference is a fraction of the interference present in the *full illumination* benchmark system: the ECDFs of the estimated and the *full illumination* benchmark scheme are of the same shape, with the estimated interference ECDF being shifted to the left. This is due to the interference estimation scheme assuming that the actual interference is a percentage of the maximum interference, whereas, in the actual system, interference is either present in full, if a beam is active, or not at all if a beam is inactive. Therefore, the interference in the proposed *adapted GEO* scheme is not accurately represented by the estimation mechanism.

The misestimation of the interference leads to poor system performance of the beam hopping scheme. In cases where the interference is under-estimated, the actual system fails to meet the user demand because the optimization does not assign enough resources to a transmission. This leads to higher outages in the proposed *adapted GEO* system. The interference is, in general, under-estimated in highly loaded networks, as most beams are activated and the full interference power is received where the interference estimation assumes that only a portion of the interference power is received.

When the interference is over-estimated, too many resources are assigned and the power consumption increases. In the worst case, the optimization problem has no valid solution and the proposed *adapted GEO* scheme defaults to full illumination.

The original GEO system [10] for which the interference estimation algorithm was designed, has an interference mitigation mechanism integrated that assures that beams that are activated simultaneously do not interfere strongly. This approach is not feasible in a LEO system at lower elevation angles, as the beam footprint is distorted and interference between the beams increases. Further, the interference estimation scheme was designed to estimate the interference of a large number of non-adjacent interfering beams, whereas it is used to estimate the interference of neighboring beams in the LEO system. The small number of interfering beams and the close proximity of the interfering beams make the probabilistic approach of the interference estimation scheme ill-suited for the LEO system.

TABLE 9. Nineteen beam simulation parameters.

Low Density	
number of users N_u	10
user demand D_u	10 Mbit/s
High Density	
number of users N_u	100
user demand D_u	{10 Mbit/s, 30 Mbit/s}

D. PERFORMANCE COMPARISON FOR NINETEEN BEAMS

In this section, the performance of the two proposed schemes, proposed *greedy* and proposed *adapted GEO*, is compared to the *random* benchmark and the *full illumination* benchmark in terms of system power consumption, user outage, and system sum rate.

For the sum rate results, an additional benchmark is compared: the full buffer system. For the full buffer results, a full illumination system with users with a full traffic buffer is considered. The benchmark is a measure for the full system capacity that is achieved when all resources in the satellite system are used. The full buffer results provide an understanding of the load under which the system is operated. When the achieved sum rate is close to the full buffer rate, all resources of the system are utilized, when the sum rate is lower, the system has a lot of unused capacity and many resources stay unutilized.

In the following, a scenario with low user density and two scenarios with high user density are analyzed. The scenario parameters are collected in Table 9. The low demand scenario showcases the performance in system under low utilization when the network has to fulfill service guarantees. The high demand scenarios showcase the behavior of the beam hopping algorithms when the network is under high load or overcrowded.

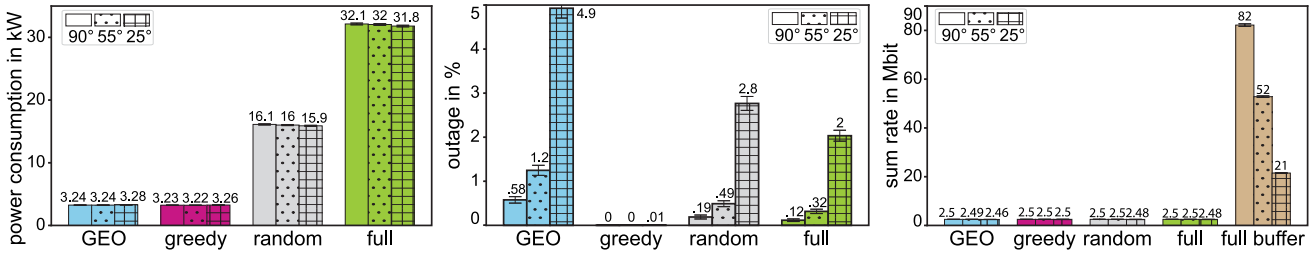

(a) Power Consumption. (b) User outage. (c) Sum rate.

FIGURE 15. Performance results with 95% confidence interval at different elevation angles for the 19 beam system with 25 users with 10 Mbit/s demand. The proposed *greedy* scheme shows good performance in a network under low load.

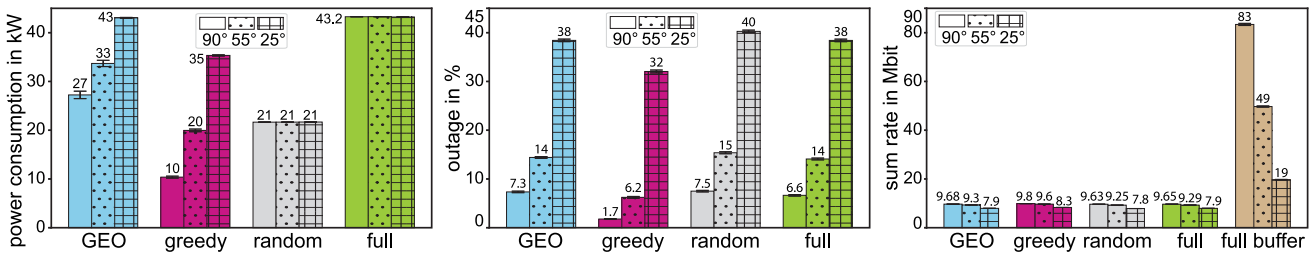

(a) Power Consumption. (b) User outage. (c) Sum rate.

FIGURE 16. Performance results with 95% confidence interval at different elevation angles for the 19 beam system with 100 users with 10 Mbit/s demand. The proposed *greedy* scheme shows good results at higher elevation angles in scenarios with a large number of users.

1) LOW USER DENSITY

The results for the low user demand scenario of the 19 beam system with 25 users with 10 Mbit/s demand each is shown in Fig. 15. Figure 15a shows the power consumption of each scheme at 90°, 55°, and 25° elevation angle. The *full illumination* benchmark results show the power consumption when all beams that have users assigned are turned on for the full beam hopping cycle. The power consumption slightly decreases with the elevation angle because the cell sizes are unevenly distributed at low elevation angles as elaborated in Section V-B.

The *random* benchmark scheme has half the power consumption since it only activates 50% of the beams. The proposed *greedy* and proposed *adapted GEO* scheme can drastically reduce the power consumption of the system to 10% of the full illumination power at high elevation angles, which corresponds to almost 90% power reduction. This shows that the potential savings when employing a beam hopping scheme are significant, which supports previous findings in [10], [44].

For both, the proposed *greedy* and the proposed *adapted GEO* scheme, the power consumption increases from 55° to 25° elevation angle. This indicates that the system struggles to fulfill the user demand at very low elevation angles and has to utilize more resources to serve the users. The difficulty of providing the desired service is also reflected in the user outage results in Fig. 15b that show higher outages at 25° elevation angle.

Despite the user outages, the system is capable of covering almost the full system demand, as can be seen in Fig. 15c. The sum rate of the system is very close to the total user demand of 2.5 Mbits in a beam hopping cycle. The good performance in terms of outage - the maximum outage rate of the proposed *greedy* scheme is 0.01% - can be explained by the low system utilization. The system is capable of providing between 21 Mbits and 82 Mbits in each beam hopping cycle, whereas the total demand is at only 2.5 Mbits per beam hopping cycle.

The results of the low demand scenario show that the proposed *greedy* scheme can reduce the power consumption by almost 90% while reducing the user outage at all elevation angles compared to all other schemes.

2) HIGH USER DENSITY

To evaluate the performance of the beam hopping schemes in a network under high load, this section compares the performance of the scheme in a network with 100 users with 10 Mbit/s and 30 Mbit/s demand. The results for the 19 beam scenario with 100 users and user demand of 10 Mbit/s are shown in Fig. 16.

The user outage in Fig. 16b increases compared to the low density case in Fig. 15b - note the adapted scale of the *y*-axis. In the low density scenario, the instantaneous outage rates were below 5%, and close to zero for the proposed *greedy*. With increased user density, the network cannot provide service guarantees anymore and the outages at 25° elevation angle are above 30%, showing that effective communication is difficult at low elevation angles.

Figure 17 shows the performance results for 100 users with an increased user demand of 30 Mbit/s, resulting in a

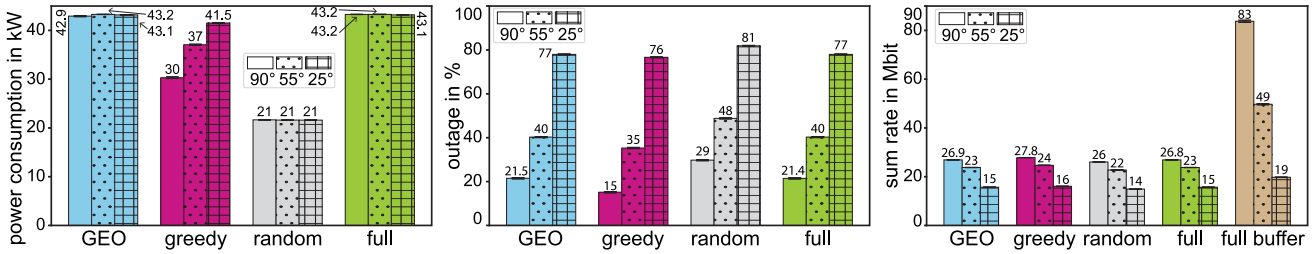

(a) Power Consumption. (b) User outage. (c) Sum rate.

FIGURE 17. Performance results with 95% confidence interval at different elevation angles for the 19 beam system with 100 users with 30 Mbit/s demand. The proposed *greedy* scheme can reduce the power consumption and outage in highly congested networks.

total user demand of 30 Mbits per beam hopping cycle. The total user demand exceeds the full buffer network capacity at 25° elevation angle, thus, the 25° elevation angle results show the performance of the beam hopping schemes under excessive network load.

The scheme that performs best under excessive network load in terms of outage and sum rate is the proposed *greedy* beam hopping scheme for which 76% of users do not get their demand met and only 16 Mbits of the total 30 Mbits are transmitted in a beam hopping cycle on average, leaving 47% of the demand unmet. The *random* benchmark beam hopping scheme has a constant power consumption that is independent of the user demand, but results in 81% outage and leaves 53% of the demand unmet.

In an overcrowded network, the *random* benchmark beam hopping scheme can be a useful approach, as it has very low computational cost and does not require channel state information, while keeping the power consumption constant. Compared to the *full illumination* benchmark scheme, the power consumption is reduced by 50%, while outage and sum rate stay almost constant. The *random* benchmark scheme is not suitable if service guarantees have to be fulfilled.

With increasing network load, the proposed *adapted GEO* beam hopping scheme degrades to the *full illumination* benchmark scheme as the number of optimization problems without a valid solution increases and the proposed *adapted GEO* scheme defaults to full illumination. In the high user demand case in Fig. 17, the performance results of the proposed *adapted GEO* and *full illumination* benchmark scheme are identical at lower elevation angles, which indicates that the optimization algorithm can never find a valid solution. This problem could be reduced by employing a different algorithm in case no solution can be found.

The proposed *greedy* approach consistently outperforms all other schemes in power consumption, outage, and sum rate. The only exception is the power consumption of the *random* benchmark scheme, which is lower in Fig. 17a, at the cost of significantly higher outage rates at high elevation angles.

E. COMPUTATIONAL COMPLEXITY

This section compares the algorithms in terms of complexity. First, the big-O time complexity is evaluated in Section V-E1. The big-O notation describes the limiting behavior of a function and is also known as Bachmann-Landau notation, or as asymptotic notation. Secondly, the computation times of the different algorithms are compared in Section V-E2.

TABLE 10. Big-O complexity of algorithms.

Algorithm	Complexity
adapted GEO	$\mathrm{O}((N_{\mathrm{beam}}N_{\mathrm{slot}})^2N_u) + N_{\mathrm{iter}}\mathrm{O}(N_{\mathrm{beam}})$
greedy	$\mathrm{O}(N_{\mathrm{beam}}N_u)(1 + N_{\mathrm{beam}}(N_{\mathrm{slot}} - 1))$
optimal	$\mathrm{O}(2^{N_{\mathrm{beam}}N_{\mathrm{slot}}})$
random	$\mathrm{O}(2N_{\mathrm{beam}} + N_{\mathrm{slot}})$
full illumination	$\mathrm{O}(1)$

1) BIG-O COMPLEXITY

The big-O complexity of the different algorithms is summarized in Table 10.

The complexity of the proposed *adapted GEO* scheme is composed of the complexity of the interference estimation algorithm $N_{\mathrm{iter}}\mathrm{O}(N_{\mathrm{beam}})$, with N_{iter} the maximum number of iterations, and the complexity of the calculation of the solution of ILP problem has a complexity of $\mathrm{O}((N_{\mathrm{beam}}N_{\mathrm{slot}})^2N_u)$ [45, Section 1.2.2].

The proposed *greedy* scheme has a complexity of $(1 + N_{\mathrm{beam}}(N_{\mathrm{slot}} - 1))\mathrm{O}(N_{\mathrm{beam}}N_u)$, where the factor $1 + N_{\mathrm{beam}}(N_{\mathrm{slot}}-1)$ represents the maximum number of iterations before convergence. The time complexity scales linearly with the number of beams N_{beam} and the number of users N_u since the algorithm loops over all beams and verifies that all users are served.

The complexity of the *optimal* benchmark algorithm is $\mathrm{O}(2^{N_{\mathrm{beam}}N_{\mathrm{slot}}})$ as it performs an exhaustive search over all possible solutions. It is possible to reduce the complexity by excluding column permutations of the beam hopping matrix from the search space. However, the time complexity of the algorithm remains exponential.

The *random* benchmark algorithm sets the beam hopping pattern for each beam in each slot, resulting in a complexity of $\mathrm{O}(N_{\mathrm{beam}} + N_{\mathrm{slot}})$. The assertion that each beam is illuminated in at least one time slot adds a loop over all N_{beam} beams, which leads to a total complexity of $\mathrm{O}(2N_{\mathrm{beam}} + N_{\mathrm{slot}})$.

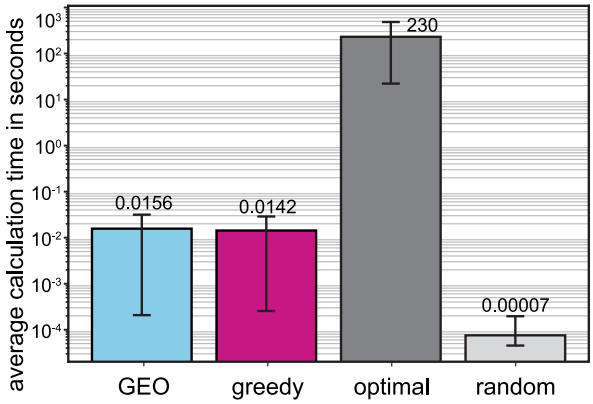

FIGURE 18. Average calculation time for different beam hopping patterns for a simulation with seven beams at 55° elevation angle and a user demand of 10 Mbit/s.

The *full illumination* benchmark algorithm does not require any computation, therefore the calculation is independent of the number of beams, time slots, or users and the complexity is constant as O(1).

When comparing the complexity of the proposed algorithms with the benchmark, we observe that the linear complexity of the proposed *greedy* algorithm is a significant improvement compared to the exponential time complexity of the *optimal* benchmark scheme. Compared to the quadratic complexity of the proposed *adapted GEO* scheme, the linear complexity of the proposed *greedy* is an improvement. This improvement is enhanced by the limited number of iterations of the proposed *greedy* with the number of iterations in practice being much lower. The maximum number of iterations of the proposed *adapted GEO* scheme can be higher.

While the big-O complexity defines how the time complexity of the algorithms scales with the size of the input parameters, the complete complexity can differ and depends on the implementation. To get a complete picture of the computational complexity, the algorithms' computation times are compared in the next section.

2) COMPUTATION TIME

The average calculation time to compute the beam hopping pattern is shown in Fig. 18 for the seven beam case with low user demand at a satellite elevation angle of 55°. A logarithmic scale is used in order to visualize the smaller computation time values. The calculation time of the *optimal* benchmark algorithm exceeds the calculation time of the proposed *adapted GEO* and proposed *greedy* algorithms by several orders of magnitude. In practice, the beam hopping pattern should be calculated for each beam hopping cycle, i.e., every 10 ms. The *optimal* benchmark search takes more than 200 s to evaluate the beam hopping pattern, showing that the *optimal* benchmark algorithm is not a viable solution for practical networks.

The proposed *adapted GEO* and proposed *greedy* algorithms show similar calculation times and can be considered equal in terms of computation time performance with the proposed *greedy* scheme showing slightly lower calculation times. It should be noted, that the main computational task in the proposed *adapted GEO* algorithm is performed using the Python-MIP package. This package is optimized for fast computation and thus little gain can be expected when the same algorithm is implemented in a practical system. The proposed *greedy* algorithm is not optimized and its calculation time can potentially be reduced to fit into a beam hopping cycle.

The *random* benchmark algorithm consistently shows calculation times below 1 ms making it suitable for practical systems in terms of complexity. Its computation time does not vary significantly with the number of users or beams. The *full illumination* benchmark algorithm is not figured in the results, as its beam hopping pattern is constant and does not require calculation.

With larger number of beams, the difference in calculation time between the proposed *greedy* algorithm and the proposed *adapted GEO* algorithm becomes larger. This is due to the increase in complexity of the optimization problem in the proposed *adapted GEO* algorithm, that affects the proposed *adapted GEO* scheme more as shown in the previous section. This trend is broken, when the network is overloaded. Then, the proposed *adapted GEO* algorithm's computation time approaches the computation time of the proposed *greedy* scheme, because the optimizer is faced with unsolvable problems, which do not require as much computation time.

In general, the calculation times of the proposed *greedy* and proposed *adapted GEO* algorithms increase when the complexity of the problem increases, i.e., when the number of beams, users, or the user demand increases. When increasing the number of beams to 19 and the number of users to 25, the computation time of the proposed *greedy* algorithm increases to about 60 ms, while the proposed *adapted GEO* algorithm takes on average 73 ms to compute. This confirms that the proposed *greedy* scales better with the number of beams than the proposed *adapted GEO* algorithm, as discussed in Section V-E1.

VI. DISCUSSION AND PERSPECTIVES

This section discusses the limitations of the presented work and presents possible extensions of the performed investigations.

The focus of this paper was the investigation of the performance of beam hopping pattern algorithms at different satellite elevation angles. Therefore, the system model applied components that have a general usability, such as the MMSE precoder and the round robin scheduler for resource allocation. The impact of these components on the system behavior is well-known, and the simulation results reflect the strengths and weaknesses of the beam hopping algorithms. To obtain optimal system performance or more realistic systems, these components could be replaced. For example, a resource allocation scheme that utilizes CSI could use

the spectral resources more efficiently and achieve higher throughput. Several works in literature treat the optimization of the beam hopping pattern and precoder design or resource allocation as a joint problem [13], [24], [46]. Replacing the MMSE precoder with a precoder that is jointly designed with the beam hopping pattern could improve the performance. The trade-off between the complexity of the joint schemes and the system's performance has not been sufficiently studied yet.

The proposed system model assumes that perfect CSI is available to determine the MMSE precoder. In practical systems, it is expected that a channel estimation error affects the available CSI due to channel fading and channel detection errors. The effect of outdated channel information on the performance is a topic for future work.

The proposed *greedy* beam hopping scheme could be further simplified by using the information about the modulation and coding scheme. If the modulation and coding scheme for a transmission is fixed before the calculation of the beam hopping matrix, the rate calculation in the proposed *greedy* algorithm could be simplified, as the number of transmitted bits is known.

To further enhance the proposed *greedy* scheme, an analysis of the convergence behavior could be performed to evaluate whether the scheme converges to local optima. If the algorithm encounters this problem, it could be extended with a randomization scheme that randomly shuffles the order in which the beams are illuminated in each iteration, which could avoid the convergence to local optima.

The channel model in this paper does not consider the Doppler shift stemming from the user's movement, the investigation of the influence of this Doppler shift is left to future work.

While co-channel interference in multi-beam satellites can be managed through beam design and beam hopping schemes, the effects of the interference from other sources need to be further investigated. Other sources include LEO satellites from the same constellation, as well as interference from other communication systems such as terrestrial networks, GEO systems, and other aerial communications systems. Further investigations could analyze whether the performance of the proposed schemes is reduced when interference from other LEO and GEO satellites is present, and whether interference from terrestrial networks impacts the performance.

When considering neighboring satellites and the design of handover schemes, future research efforts should investigate joint beam design. The beam steering capabilities of large antenna arrays mounted on satellites are not fully employed yet. Beam steering can help increase receive power and reduce interference, especially when combined with a beam hopping scheme. The analog precoder could steer the beams towards the users served by this satellite and away from users served by neighboring satellites instead of using a fixed beam steering scheme. The increased antenna gain and reduced interference would improve the link budget of the system, leading to lower transmit powers and possibly less interference.

To confirm the applicability of our findings on practical systems, the performance analysis presented in this work should be validated through experiments in an operational satellite environment.

This study is performed for a satellite altitude of 600 km. Very low altitude satellites operating at altitudes below 400 km and medium Earth orbit satellites operating at altitudes between 2000 km and 35786 km will be in operation in future communication systems, but likely present a different angle-dependent behavior. The investigation of very low and medium Earth orbit systems is left for future investigation.

VII. CONCLUSION

Beam hopping patterns increase resource efficiency in GEO satellite systems. With the widespread adoption of LEO satellite networks, the adaptation and evaluation of GEO beam hopping algorithms in LEO satellite systems is of interest. One additional challenge in LEO satellites compared to GEO is the change of the system behavior with changing elevation angle of the satellite. The elevation angle dependence of beam hopping pattern performance has not sufficiently been studied so far. To offer insights into the elevation angle-dependent behavior of beam hopping methods, the performance of five methods is compared at three representative elevation angles.

This paper newly designs two beam hopping methods. Firstly, by adapting an existing beam hopping scheme from GEO systems and secondly, by proposing an interference-aware greedy beam hopping scheme for downlink LEO satellite communication in the K_a-band (30 GHz). The proposed methods are compared to three benchmark schemes: random, full illumination, and optimal exhaustive search. For power consumption analysis, we derive a power consumption model for downlink LEO satellite transmission.

Numerical evaluations show that the proposed interference-aware greedy approach can simultaneously reduce the system's power consumption and user outages compared to the benchmarks and the proposed adaptation of the GEO scheme. The beam hopping scheme can reduce the power consumption of the system by almost 90% in a network operated at low capacity compared to the full illumination case. In crowded and overcrowded networks, the proposed greedy approach outperforms the other schemes, offering a power consumption reduction of 7% in a fully utilized network.

The adapted GEO beam hopping scheme shows poor performance as it relies on an interference estimation algorithm that is not suited for LEO satellite communication systems that suffer from strong co-channel interference. This result indicates that schemes developed for GEO systems cannot be directly applied to LEO systems but require adjustment to the additional challenges faced in a LEO satellite system stemming from the rapid movement of the satellite.

The performance results also indicate that low satellite elevation angles of 25° are challenging to use for reliable transmission. As trade-off needs to be found between high handover rates and the operation of the system under low satellite elevation angles.

Finally, the limitations of this work and future research perspectives were discussed, namely in terms of joint precoding/resource allocation/beam hopping optimization, beam steering and mitigation of interference from other satellites, as well as extensions towards inter-satellite handovers and very low Earth orbit systems.

APPENDIX

A. UNIFORM DISTRIBUTION OF POINTS IN A SECTION OF A SPHERE

We can derive the distribution of points on a section of a sphere from the commonly known uniform distribution of points P on a sphere. The points are generated in a spherical coordinate system where the sphere radius is set to r, the azimuth angle ϕ_p of a point is drawn from a uniform distribution $\phi_p \sim U(0, 2\pi)$, and the elevation angle θ_P can be generated with $\theta_U \sim U(0, 1)$ as

$$\theta_P = \arccos(1 - 2\theta_U). \tag{42}$$

To obtain the points on only a section of the sphere, the range of the elevation angles θ_P needs to be limited to the interval $[0, \theta_{\text{lim}}]$, where θ_{lim} is the maximum desired elevation angle as sketched in Fig. 2. We can find a range for θ_U starting from

$$\arccos(1 - 2\theta_U) \in [0, \theta_{\text{lim}}], \tag{43}$$

where, we can apply the $\cos(\cdot)$ function and obtain

$$1 - 2\theta_U \in [\cos(\theta_{\text{lim}}), 1]. \tag{44}$$

By further multiplying by -1, which swaps the upper and lower bounds, and shifting the additive terms to the limits, we finally obtain

$$\theta_U \in [0, 0.5 - 0.5\cos(\theta_{\text{lim}})]. \tag{45}$$

With this, the points can be generated by replacing the bounds of the uniform distribution of the elevation angles on a sphere with $\theta_U \sim U(0, 0.5 - 0.5\cos(\theta_{\text{lim}}))$ and then calculating $\theta_P = \arccos(1 - 2\theta_U)$.

The expression for θ_P can further be simplified, when plugging in the new limits of the uniform distribution used to generate θ_U into the elevation angle generation function $\arccos(1 - 2\theta_U)$. We start with plugging in the lower bound 0 for θ_U to obtain

$$\arccos(1 - 2\theta_U) = \arccos(1 - 2 \cdot 0) = \arccos(1). \tag{46}$$

For the upper bound, we obtain

$$\arccos(1 - 2\theta_U) = \arccos(1 - 2(0.5 - 0.5\cos(\theta_{\text{lim}}))) \tag{47}$$

$$= \arccos(\cos(\theta_{\text{lim}})). \tag{48}$$

This finally leaves us with

$$\theta_P \sim \arccos(U(\cos(\theta_{\text{lim}}), 1)), \tag{49}$$

for the generation of the elevation angle of points distributed uniformly at random in a section of a sphere, which corresponds to (2).

In summary, the point generation function for uniformly distributed points on the pole section defined by angle θ_{lim} of a sphere of radius r_{Earth} in spherical coordinates (r, θ, ϕ) can be denoted as

$$r = r_{\text{Earth}} = 6371 \text{ km}, \tag{50}$$

$$\theta \sim \arccos(U(\cos(\theta_{\text{lim}}), 1)), \tag{51}$$

$$\phi \sim U(0, 2\pi). \tag{52}$$

B. THE ANTENNA ARRAY STEERING VECTOR

The phase shift vector $\mathbf{a}_u^{(X)} \in \mathbb{C}^{1\times n_x}$ of a uniform linear array with antenna elements positioned in a row in x-direction is

$$\mathbf{a}_u^{(X)} = \frac{1}{\sqrt{n_x}}\left[e^{jx\pi\Phi_x^{(u)}}, e^{j(x+1)\pi\Phi_x^{(u)}}, \ldots, e^{j(x+n_x-1)\pi\Phi_x^{(u)}}\right], \tag{53}$$

where $x = (X-1)n_x$ is the index of the first antenna element of the panel at position X. The factor $\frac{1}{\sqrt{n_x}}$ normalizes the phase shift vector, as we are modeling a passive system component that should not apply a power gain.

$$\Phi_x^{(u)} = \sin(\theta_u)\cos(\phi_u) \tag{54}$$

represents the phase shift induced by the transmission delay of the signal traveling over the additional distance introduced by the antenna element spacing. The angles ϕ_u and θ_u are the azimuth and elevation angle between antenna array and the user defined in Fig. 2.

In a similar fashion, the phase shift vector $\mathbf{a}_u^{(Y)} \in \mathbb{C}^{1\times n_y}$ of a uniform linear array with antenna elements positioned in a column in y-direction is modeled as

$$\mathbf{a}_u^{(Y)} = \frac{1}{\sqrt{n_y}}\left[e^{jy\pi\Phi_y^{(u)}}, e^{j(y+1)\pi\Phi_y^{(u)}}, \ldots, e^{j(y+n_y-1)\pi\Phi_y^{(u)}}\right], \tag{55}$$

with $y = (Y-1)n_y$ being the index of the first antenna element in y-direction of the panel and the phase shift induced by the antenna spacing

$$\Phi_y^{(u)} = \sin(\theta_u)\sin(\phi_u). \tag{56}$$

ACKNOWLEDGMENT

This work was performed while Younes El Hadfi was an internship student at the National Institute of Informatics, Tokyo, Japan.

REFERENCES

[1] H. Shahid et al., "Emerging advancements in 6G NTN radio access technologies: An overview," in *Proc. Joint Eur. Conf. Netw. Commun. 6G Summit (EuCNC/6G Summit)*, Jun. 2024, pp. 593–598.

[2] M. Y. Abdelsadek, G. Karabulut-Kurt, H. Yanikomeroglu, P. Hu, G. Lamontagne, and K. Ahmed, "Broadband connectivity for handheld devices via LEO satellites: Is distributed massive MIMO the answer?" *IEEE Open J. Commun. Soc.*, vol. 4, pp. 713–726, 2023.

[3] F. Michel, M. Trevisan, D. Giordano, and O. Bonaventure, "A first look at starlink performance," in *Proc. 22nd ACM Internet Meas. Conf.*, Oct. 2022, pp. 130–136.

[4] *Series G: Transmission Systems and Media, Digital Systems and Networks—International Telephone Connections and Circuits—General Recommendations on the Transmission Quality for an Entire International Telephone Connection: One-Way Transmission Time*, Int. Telecommun. Union, Geneva, Switzerland, Rec. G.114, May 2003.

[5] E. Kim, I. P. Roberts, and J. G. Andrews, "Downlink analysis and evaluation of multi-beam LEO satellite communication in shadowed Rician channels," *IEEE Trans. Veh. Technol.*, vol. 73, no. 2, pp. 2061–2075, Feb. 2024.

[6] L. M. Marrero et al., "Differential phase compensation in over-the-air precoding test-bed for a multi-beam satellite," in *Proc. IEEE Wireless Commun. Netw. Conf. (WCNC)*, Apr. 2022, pp. 1325–1330.

[7] K.-U. Storek, R. T. Schwarz, and A. Knopp, "Multi-satellite multi-user MIMO precoding: Testbed and field trial," in *Proc. IEEE Int. Conf. Commun. (ICC)*, Jun. 2020, pp. 1–7.

[8] S. Tadavarty and N. K. Chavali, "Estimation and compensation of doppler in 5G NR based non-terrestrial networks," in *Proc. IEEE Int. Conf. Adv. Netw. Telecommun. Syst. (ANTS)*, Dec. 2022, pp. 135–140.

[9] A. Fastenbauer, M. Kaneko, P. Svoboda, and M. Rupp, "Impact of elevation angle on multi-beam LEO satellite communication systems," *IEEE Access*, vol. 13, pp. 71723–71737, 2025.

[10] L. Chen, V. N. Ha, E. Lagunas, L. Wu, S. Chatzinotas, and B. Ottersten, "The next generation of beam hopping satellite systems: Dynamic beam illumination with selective precoding," *IEEE Trans. Wireless Commun.*, vol. 22, no. 4, pp. 2666–2682, Apr. 2023.

[11] V. N. Ha, T. T. Nguyen, E. Lagunas, J. C. M. Duncan, and S. Chatzinotas, "GEO payload power minimization: Joint precoding and beam hopping design," in *Proc. IEEE Global Commun. Conf.*, Dec. 2022, pp. 6445–6450.

[12] Z. Han, T. Yang, and R. Liu, "On beam hopping pattern design for satellite communication systems with hybrid precoding," *IEEE Trans. Veh. Technol.*, vol. 73, no. 1, pp. 1364–1369, Jan. 2024.

[13] J. Wang, C. Qi, S. Yu, and S. Mao, "Joint beamforming and illumination pattern design for beam-hopping LEO satellite communications," *IEEE Trans. Wireless Commun.*, vol. 23, no. 12, pp. 18940–18950, Dec. 2024.

[14] E. Meng, J. Yu, S. Jin, X. Bu, and J. An, "Resource allocation for MC-DS-CDMA in beam-hopping LEO satellite networks," *IEEE Trans. Aerosp. Electron. Syst.*, vol. 60, no. 3, pp. 3611–3624, Jun. 2024.

[15] A. I. Perez-Neira, M. A. Vazquez, M. B. Shankar, S. Maleki, and S. Chatzinotas, "Signal processing for high-throughput satellites: Challenges in new interference-limited scenarios," *IEEE Signal Process. Mag.*, vol. 36, no. 4, pp. 112–131, Jul. 2019.

[16] M. A. Vazquez et al., "Precoding, scheduling, and link adaptation in mobile interactive multibeam satellite systems," *IEEE J. Sel. Areas Commun.*, vol. 36, no. 5, pp. 971–980, May 2018.

[17] J. Anzalchi et al., "Beam hopping in multi-beam broadband satellite systems: System simulation and performance comparison with non-hopped systems," in *Proc. 5th Adv. Satell. Multimedia Syst. Conf. 11th Signal Process. Space Commun. Workshop*, Sep. 2010, pp. 248–255.

[18] V. K. Gupta, V. N. Ha, E. Lagunas, H. Al-Hraishawi, L. Chen, and S. Chatzinotas, "Combining time-flexible GEO satellite payload with precoding: The cluster hopping approach," *IEEE Trans. Veh. Technol.*, vol. 72, no. 12, pp. 16508–16523, Dec. 2023.

[19] X. Hu, L. Wang, Y. Wang, S. Xu, Z. Liu, and W. Wang, "Dynamic beam hopping for DVB-S2X GEO satellite: A DRL-powered GA approach," *IEEE Commun. Lett.*, vol. 26, no. 4, pp. 808–812, Apr. 2022.

[20] S. Sharma, S. Han, J. Seong, and W. Shin, "Cluster hopping in multi-beam satellite communication systems using deep reinforcement learning," in *Proc. 14th Int. Conf. Inf. Commun. Technol. Converg. (ICTC)*, Oct. 2023, pp. 412–414.

[21] W. Li, M. Zeng, X. Wang, and Z. Fei, "Dynamic beam hopping of double LEO multi-beam satellite based on determinant point process," in *Proc. 14th Int. Conf. Wireless Commun. Signal Process. (WCSP)*, Nov. 2022, pp. 713–718.

[22] Y. Han, C. Zhang, and G. Zhang, "Dynamic beam hopping resource allocation algorithm based on deep reinforcement learning in multi-beam satellite systems," in *Proc. 3rd Int. Academic Exchange Conf. Sci. Technol. Innov. (IAECST)*, Dec. 2021, pp. 68–73.

[23] R. Zhao, J. Cai, J. Luo, J. Gao, and Y. Ran, "Demand-aware beam hopping and power allocation for load balancing in digital twin empowered LEO satellite networks," *IEEE Trans. Wireless Commun.*, vol. 24, no. 6, pp. 5084–5098, Jun. 2025.

[24] M. Meng, B. Hu, S. Chen, and S. Kang, "Joint beamforming and dynamic beam hopping based on MAPPO for LEO satellite communication system," *IEEE Wireless Commun. Lett.*, vol. 14, no. 5, pp. 1461–1465, May 2025.

[25] C. Zhang, L. Qu, P. Liu, and N. Li, "Beam hopping and power allocation method for multi-beam satellite system based on heterogeneous graph," in *Proc. 2nd Int. Conf. Artif. Intell. Autom. Control (AIAC)*, Dec. 2024, pp. 422–426.

[26] *IEEE Standard Letter Designations for Radar-Frequency Bands*, IEEE Standard 521-1976, 1976.

[27] R. Mendez-Rial, C. Rusu, N. Gonzalez-Prelcic, A. Alkhateeb, and R. W. Heath, "Hybrid MIMO architectures for millimeter wave communications: Phase shifters or switches?" *IEEE Access*, vol. 4, pp. 247–267, 2016.

[28] T. H. Lee, *The Design of CMOS Radio-Frequency Integrated Circuits*, 2nd ed. Cambridge, U.K.: Cambridge Univ. Press, 2009.

[29] A. Enqvist, O. T. Demir, C. Cavdar, and E. Björnson, "Fundamentals of energy-efficient wireless links: Optimal ratios and scaling behaviors," in *Proc. 99th IEEE Veh. Technol. Conf. (VTC)*, Jul. 2024, pp. 1–6.

[30] L. You et al., "Hybrid analog/digital precoding for downlink massive MIMO LEO satellite communications," *IEEE Trans. Wireless Commun.*, vol. 21, no. 8, pp. 5962–5976, Aug. 2022.

[31] A. Fastenbauer, Y. El Hadfi, M. Kaneko, P. Svoboda, and M. Rupp, "Multi-beam LEO satellite beam hopping framework," 2025. [Online]. Available: https://researchdata.tuwien.ac.at/records/8e0pf-6qz94

[32] "Technical specification group radio access network; study on new radio (NR) to support non-terrestrial networks (Release 15) V15.4.0," 3GPP, Sophia Antipolis, France, Rep. TR 38.811, Sep. 2020.

[33] S. M. Zamacola, R. M. Rodríguez-Osorio, and M. A. Salas-Natera, "Joint satellite platform and constellation sizing for instantaneous beam-hopping in 5G/6G non-terrestrial networks," *Comput. Netw.*, vol. 257, Feb. 2025, Art. no. 110942.

[34] Z. Shuang, Z. Xing, W. Peng, and W. Wenbo, "Joint beam scheduling and power optimization for beam hopping LEO satellite systems," *China Commun.*, vol. 21, no. 10, pp. 1–14, Oct. 2024.

[35] C. A. Balanis, *Antenna Theory: Analysis and Design*, 1st ed. New York, NY, USA: Wiley, 2016.

[36] J. Heo, S. Sung, H. Lee, I. Hwang, and D. Hong, "MIMO satellite communication systems: A survey from the PHY layer perspective," *IEEE Commun. Surveys Tuts.*, vol. 25, no. 3, pp. 1543–1570, 3rd Quart., 2023.

[37] C. Mosquera, R. Lopez-Valcarce, T. Ramirez, and V. Joroughi, "Distributed precoding systems in multi-gateway multibeam satellites: Regularization and coarse beamforming," *IEEE Trans. Wireless Commun.*, vol. 17, no. 10, pp. 6389–6403, Oct. 2018.

[38] J. Krivochiza et al., "End-to-end precoding validation over a live GEO satellite forward link," *IEEE Access*, vol. 11, pp. 41556–41564, 2023.

[39] "Python-MIP," Dept. Comput. Federal, Univ. Ouro Preto, Ouro Preto, Brazil, Jul. 2024. [Online]. Available: https://www.python-mip.com/

[40] "Technical specification group radio access network; solutions for NR to support non-terrestrial networks (NTN) V16.2.0," 3GPP, Sophia Antipolis, France, Rep. TR 38.821, Mar. 2023.

[41] I. del Portillo, "ITU-Rpy," 2017. [Online]. Available: https://github.com/inigodelportillo/ITU-Rpy/

[42] M. Mahmood, A. Koc, and T. Le-Ngoc, "Energy-efficient MU-massive-MIMO hybrid precoder design: Low-resolution phase shifters and digital-to-analog converters for 2D antenna array structures," *IEEE Open J. Commun. Soc.*, vol. 2, pp. 1842–1861, 2021.

[43] C. Chen, Y. Dong, X. Cheng, and L. Yang, "Low-resolution PSs based hybrid precoding for multiuser communication systems," *IEEE Trans. Veh. Technol.*, vol. 67, no. 7, pp. 6037–6047, Jul. 2018.
[44] P. Eberechukwu N., M. Onyekwelu, and D. Yoon, "Extended DL coverage in SAGIN: Cell association and resource allocation with beam hopping LEO," *IEEE Internet Things J.*, vol. 12, no. 5, pp. 6014–6028, Mar. 2025.
[45] S. P. Boyd and L. Vandenberghe, *Convex Optimization*. Cambridge, U.K.: Cambridge Univ. Press, 2009.
[46] L. Chen et al., "Joint power allocation and beam scheduling in beam-hopping satellites: A two-stage framework with a probabilistic perspective," *IEEE Trans. Wireless Commun.*, vol. 23, no. 10, pp. 14685–14701, Oct. 2024.

AGNES FASTENBAUER (Member, IEEE) received the B.Sc. degree in electrical engineering in 2019, and the Dipl.-Ing. degree in telecommunications from TU Wien, Austria, in 2021, where she is currently pursuing the Doctoral degree, under supervision of Prof. M. Rupp.

In 2024, she completed an internship with the National Institute of Informatics, Tokyo, Japan, under the supervision of Prof. M. Kaneko. Her focus is on system-level evaluation and simulation of multitier wireless networks.

YOUNES EL HADFI received the Diplôme d'ingénieur degree in informatics and telecommunication from Toulouse-INP ENSEEIHT, France, in 2023, jointly with a master's degree in advanced communication systems from ISAE-Supaero, France, where he is currently pursuing the Ph.D. degree, under the supervision of Prof. W. Martins.

In 2023, he completed a Research Internship with the National Institute of Informatics in Tokyo, Japan, under the supervision of Prof. M. Kaneko. His focus is on wideband beamforming, distributed beamforming and satellites swarms.

MEGUMI KANEKO (Senior Member, IEEE) received the Diplôme d'Ingénieur degree from Télécom SudParis (French Grande Ecole), France, in 2004, jointly with a M.Sc. degree degree from Aalborg University, Denmark, the Ph.D. degree from Aalborg University in 2007, and the HDR degree (French Doctoral Habilitation for Directing Researches at Professor position) from Paris-Saclay University, France, in May 2017.

From April 2008 to August 2010, she was a JSPS Postdoctoral Fellow with Kyoto University, where she was an Assistant Professor with the Department of Systems Science, Graduate School of Informatics from September 2010 to March 2016. From April 2016 to March 2024, she was an Associate Professor with the National Institute of Informatics (NII) as well as the Graduate University for Advanced Studies (Sokendai), Tokyo, Japan. She is currently a Full Professor with NII and also with the University of Tokyo. Her research interests include wireless communications, PHY/MAC design and optimization, energy efficiency, and IoT massive connectivity.

Prof. Kaneko received multiple awards among which the 2009 Ericsson Young Scientist Award, the IEEE Globecom 2009 Best Paper Award, the WPMC 2011 Best Paper Award, the 2012 Telecom System Technology Award, the 2019 Young Scientist Prize from the Minister of Education, Culture, Sports, Science and Technology of Japan, the 2020 IEEE Communications Letters Exemplary Editor Award, and the 2021 KDDI Foundation Contributions Award. She serves as an Editor for IEEE TRANSACTIONS ON WIRELESS COMMUNICATIONS, IEEE COMMUNICATIONS LETTERS, and IEEE WIRELESS COMMUNICATIONS LETTERS. Since September 2020, she has been a member of the Advisory Board for Promoting Science and Technology Diplomacy at the Ministry of Foreign Affairs of Japan.

PHILIPP SVOBODA (Senior Member, IEEE) received the Dr.Ing. degree in electrical engineering from TU Wien, Austria, in 2008.

He is a Senior Scientist with TU Wien, with a research focus on the performance aspects of mobile cellular technologies. He is currently examining the feasibility of using crowdsourcing to conduct performance measurements on 4G and 5G mobile networks. His research aims to establish a common framework for evaluating the performance of mobile networks, guaranteeing reliable, and fair connectivity for end-users.

MARKUS RUPP (Fellow, IEEE) received the Dipl.-Ing. degree from the University of Saarbrücken, Germany, in 1988, and the Dr.-Ing. degree from the Technische Universität Darmstadt, Germany, in 1993.

Until 1995, he was a Postdoctoral Fellow with the University of California at Santa Barbara. From 1995 until 2001, he was a Technical Staff Member with the Wireless Technology Research Department, Bell-Labs, Crawford Hill, NJ, USA. Since October 2001, he has been a Full Professor of Digital Signal Processing in Mobile Communications with TU Wien, Austria.